Electrochemical Materials and Technologies

REVIEW

Electrochemical Materials and Technologies

eISSN:

Cite this: Electrochem. Mater. Technol. 1 (2022) 20221006

Solid Oxide Fuel Cells with a Thin Film Electrolyte: A Review on Manufacturing Technologies and Electrochemical Characteristics

Liliya Dunyushkina[a]

Received: 10 August 2022
Accepted: 10 September 2022

DOI: 10.15726/elmattech.2022.1.006

Solid oxide fuel cells (SOFCs) are electrochemical systems converting the energy released during fuel oxidation into electrical energy. SOFCs are considered as a promising clean energy technology due to the high efficiency of fuel-to-power conversion and environmental friendliness. The potential applications of SOFCs extend from stationary power generation units for industrial and household facilities to auxiliary power units in vehicles and portable power sources. One of the main elements of SOFCs is a solid oxide electrolyte possessing ionic conductivity at high temperatures (above 700 °C). The main challenge in the SOFC commercialization is related to their high operating temperature, which entails materials degradation, short life-time, long start-up and shut-down times, and high cost. One of the most effective ways to reduce the SOFC operating temperature is to minimize the electrolyte thickness. In this regard, fabrication of SOFCs with a thin film electrolyte has been attracting high research activity over the past few decades. Different fabrication techniques were reported to be applicable for manufacturing thin film SOFCs, and the fuel cell performance was found to be highly dependent on the appropriate selection of materials and processing technologies. The present review is focused on state-of-the-art fabrication technologies of the thin film SOFCs. A brief survey of configurations and geometries of the thin film SOFCs and methods of deposition of solid-oxide films is given. Special attention is focused on the electrical generation performance of the thin film SOFCs.

keywords: electrode-supported SOFC, metal-supported SOFC, thin film electrolyte, film deposition, freestanding electrolyte

1. Introduction

Fuel cells generate clean energy in an efficient and reliable way. Solid oxide fuel cells (SOFCs) are considered to be the most promising fuel cell technology among other types of fuel cells (proton-exchange membrane-, direct methanol-, alkaline-, phosphoric acid- and molten carbonate fuel cells) due to their exceptionally high efficiency, especially when the SOFC operation is combined with a heat source [1–4]. Application of SOFCs for energy production is an effective way to reduce the negative impact of existing energy technologies, especially considering the issue of high greenhouse gas emission. Besides, SOFCs are flexible with respect to fuel

a: Institute of High Temperature Electrochemistry, Ural Division of Russian Academy of Sciences, Ekaterinburg 620066, Russia

* Corresponding author: l_dun@ihte.uran.ru

selection, being able to operate on a variety of fuels – including natural gas, biogas, hydrogen, hydrocarbons, syngas etc. [5–7]. Due to the high operation temperature (700–1000°C), the internal reforming of light hydrocarbons (e.g. methane) is feasible in SOFCs, which eliminates the need for pre-reformers and allows for the cost reduction [8-11]. The other advantage of high operating temperature is that there is no need to use expensive precious metals as a catalyst, in contrast to the proton-exchange membrane fuel cells; instead, more affordable oxides or composite materials possessing high electrochemical activity at high temperatures can be used in SOFCs [12-16]. SOFCs may find application in a wide range of areas, including stationary power generation for industrial and household facilities, auxiliary power units in vehicles, power supply in all-electric vehicles and portable electronic apparatus. The use of SOFCs as a part of a combined heat and power system, where the excess thermal energy from the fuel cell is used for space and water heating, increases the overall system efficiency.

Despite the obvious advantages of SOFCs, their high operation temperature leads to a number of difficulties such as time-consuming start-up and shut-down procedures, materials degradation, short lifespan and high cost. The increasing variety of portable electronic devices such as cellular phones, notebooks, laptops, military and medical apparatus etc., has set the ground for the development of low-sized SOFCs operating at intermediate temperatures in order to provide the necessary energy supply [2,5,7,17,18]. In contrast to batteries, which need periodic recharges, the fuel cells produce power permanently, as long as fuel and air are supplied. Consequently, the current trend in the SOFC technology development is directed at reducing operating temperature and weight-size parameters of the fuel cells. The most evident solutions of these problems include searching for novel highly conductive and electrochemically active materials, decreasing thickness and optimizing microstructure of the functional layers. Fabrication of SOFCs with a thin film electrolyte has been attracting high research activity over the past few decades; and the present review aims to summarize the current challenges and advantages in this field, including fabrication technologies, design strategies, and electricity generation performances.

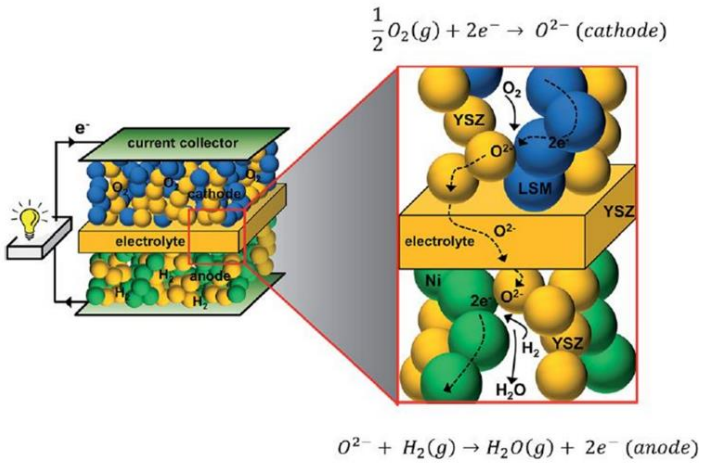

Figure 1 Schematic diagram of a hydrogen fueled SOFC and its operation mechanism [19].

2. Operation mechanism, configurations and geometries of thin film SOFCs

A typical SOFC is composed of two porous ceramic electrodes separated by a dense solid oxide electrolyte. Schematic structure and operation mechanism of SOFCs are presented in Figure 1. Gaseous fuel (in the present case, hydrogen) is fed to the anode side, while the air is supplied to the cathode side. The difference of the oxygen chemical potentials in the anode and cathode gases creates a driving force for reduction of oxygen into oxide ions at the cathode and diffusion of the oxide ions through the solid oxide electrolyte to the anode, where they oxidize the fuel. Accordingly, the electrons are generated at the anode and flow toward the cathode through an external circuit. Thus, chemical energy is converted to electrical energy.

Yttria-stabilized zirconia (YSZ) with a fluorite structure is the most commonly used electrolyte due to its excellent electrolytic properties, chemical stability, and mechanical strength [20-22]. The history of SOFCs began with the electrolyte-supported cells due to the excellent mechanical properties of YSZ ceramics. Later, other oxide-ion electrolytes, such as CeO2 based oxides with the fluorite structure, LaGaO3 based perovskites etc., and the proton-conducting electrolytes began to be used [13,14]. The fact that the oxide-ion conductivity in solid oxide electrolytes reaches a sufficient value at the temperatures above 700°C determines the range of the SOFC operating temperatures (700–1000°C). The use of proton-conducting electrolytes allows for the reduction of the SOFC temperature to 500–700°C due to the lower activation energy of proton transport. A porous cermet

made of nickel and YSZ or another electrolyte is generally used in SOFCs as an anode [19,23-26]. The ceramic component in the cermet anode smoothes the chemical and thermal mismatch of the electrode and electrolyte materials, which is crucial for the SOFC integrity [27]. Solid oxides possessing high oxide-ion and electronic conduction are considered as suitable cathode materials; the most commonly used among them are the oxides AMO_3 (A = La, Ba, Sr; M= Mn; Fe, Co, Ni) with the perovskite-type structure [19,28-33] and A_2NiO_4 (A = La, Nd, Pr or Sr) with the Ruddlseden-Popper structure [34–38].

The main configurations of the thin film SOFCs are the cells with (i) a supporting electrolyte, (ii) a supporting electrode (an anode or a cathode), and (iii) an external support [39], as schematically shown in Figure 2. The SOFC with a freestanding electrolyte film, which is schematically presented in Figure 3, can be considered as a distinct type of thin film SOFCs [39,40]. In the case of the electrolyte-supported SOFC, a dense ceramic electrolyte provides mechanical support of the cell. For this purpose, the electrolyte thickness should be at least 200 μm, which causes significant ohmic losses during SOFC operation. Currently, the most common types of thin film SOFCs are the anode- and metal-supported ones. Cathode-supported SOFCs are less frequent because of a significant mismatch of thermal behavior of the materials. In addition, the need for high-temperature sintering of an electrolyte film leads to chemical reactions of the electrolyte with common cathode materials.

The main SOFC geometries are planar and tubular; their schematic views are depicted in Figure 4. The planar cell is a typical sandwich geometry with a planar electrolyte membrane placed between electrodes. This geometry is commonly used due to the relatively simple and low-cost manufacturing technology of single cells and high density of power; however, the assembling of single cells in a stack and the stack hermetization are rather sophisticated [39–43]. In contrast to the planar cells, the tubular geometry provides much easier sealing and hermetization of stacks, but manufacturing of single cells is more complicated.

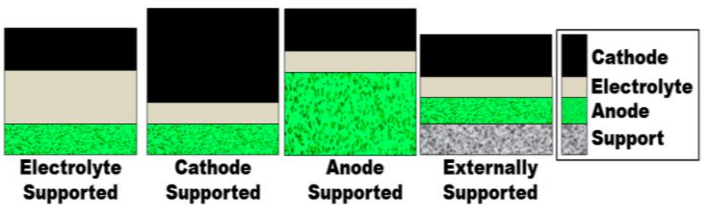

Figure 2 Schematic configurations of the film-supported SOFCs [39].

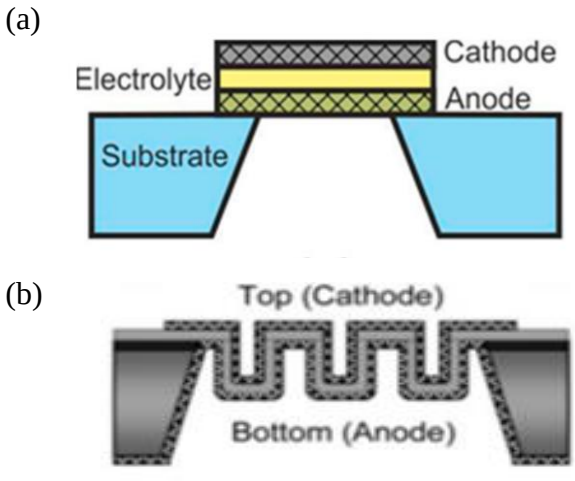

Figure 3 Schematic configurations of a SOFC with a freestanding electrolyte: (a) flat cell [40], (b) corrugated cell [41].

3. Brief description of film deposition technologies

Film deposition technologies can be divided into three groups: the methods based on (i) physical processes (physical vapor deposition, PVD), (ii) chemical processes (chemical vapor deposition (CVD) and chemical solution deposition (CSD)), and (iii) ceramic powder-based technologies [44-49].

PVD includes vaporization or sputtering of a solid target in a vacuum and deposition of the vaporized particles on a substrate surface [50-52]. High vacuum conditions are required to ensure transport of the film-forming particles to the substrate without losing energy by colliding with gas atoms. A large variety of PVD techniques such as electron beam physical vapor deposition [53-56], ion beam sputtering [57,58], magnetron sputtering [59-61] were shown to be applicable for film deposition of solid oxide electrolytes.

CVD technologies are based on deposition of gaseous precursors on a substrate surface, followed by chemical interaction to produce a film of a target composition [62]. The gas phase can be generated by spraying (Aerosol Assisted CVD, Spray Pyrolysis) [63,64] or injection of liquid solutions (Direct Liquid Injection) [65]. Atomic layer deposition (ALD) is a variant of the CVD technology based on alternation of two or more sequential surface reactions of gaseous precursors; each surface reaction is completed by formation of one atomic layer bound with the underlying layer by chemical bonds [66-69].

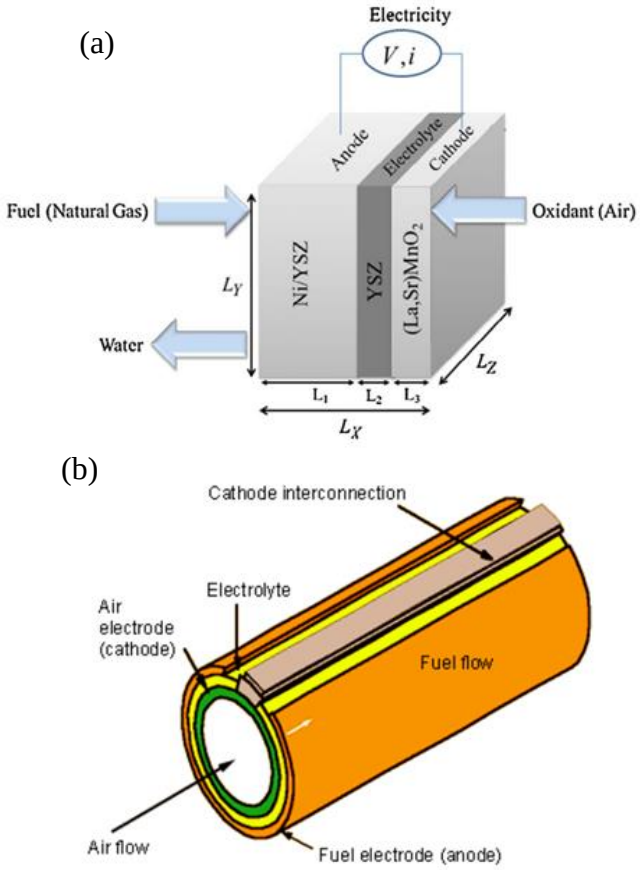

Figure 4 Schematic views of (a) planar and (b) tubular SOFCs [41,43].

Deposition of alternating monolayers results in the formation of an epitaxial film of a target composition. CVD and PVD technologies male it possible to obtain films with a thickness from a few nanometers to hundreds of nanometers.

CSD methods are based on deposition of liquid solutions containing film-forming cations on a substrate surface, followed by chemical reactions to produce a target film [70-73]. The film-forming solution is typically deposited on a substrate surface by multi-step spin-coating, dip-coating or spraying; then the deposited layer is exposed to drying and synthesis. Thickness of the films produced by CSD depends on the solution characteristics (concentration, viscosity, wetting ability), the substrate surface state (roughness, porosity), and the deposition process parameters, however, after a single deposition step, it typically reaches tens of nanometers [73]. To attain sufficient gas-tightness of the film membrane, several steps of solution deposition are typically required.

The ceramic powder-based technologies are used for fabrication of ceramic layers with a thickness of several micrometers. Most of the ceramic powder-based methods are based on casting of a suspension, or a slurry, which contains a fine oxide powder, a solvent, a binder, a dispersant, a plasticizer, and other components. The commonly used methods of the ceramic slurry casting are tape-casting [74-77], tape-calendaring [78-80], screen-printing [81-85], and phase inversion [86-88]. Electrophoretic deposition, in which fine ceramic particles suspended in a liquid medium migrate to an electrode, forming a coating under an applied electric field, also can be considered the ceramic powder-based technique [89-93]. The suspension composition and the processing parameters must be thoroughly developed for each composition and casting technology of the produced ceramic layer. The powder-based methods are technologically simple, cost-effective, and scalable; that is why they are widely used in the SOFC manufacturing.

4. Anode-supported SOFCs

4.1 Fabrication and performance of planar type anode supported SOFCs

The planar anode-supported SOFCs are considered to be a promising type of thin film SOFCs due to the lowered ohmic losses, which allows for the enhancement of the cell efficiency, relatively low-cost and scalable manufacturing processes. The fabrication technologies and performance of the planar anode-supported fuel cells have been reported in multiple studies. The technologies based on the use of ceramic powders are widely used for casting of oxide- and composite functional layers for SOFCs due to their high scalability and low cost.

A fuel cell with a thin proton conducting electrolyte $SrZr_{0.5}Ce_{0.4}Y_{0.1}O_{3-\delta}$ (SZCY) supported by NiO–SZCY (weight ratio of 3:2) composite anode and $BaCo_{0.4}Fe_{0.4}Zr_{0.1}Y_{0.1}O_{3-\delta}$ (BCFZY) cathode was fabricated by using tape-casting and screen-printing techniques by Leonard et al. [95]. First, the slurry containing the SZCY ceramic powder was cast onto a silicone-coated polymeric foil and dried at room temperature, then a thin functional layer of NiO–SZCY slurry was cast directly on the SZCY layer and dried, and lastly the support layer of NiO–SZCY slurry was cast over the functional layer and properly dried. This 3-layered green tape was cut into square plates and sintered at 1300 °C for 5 h. Flat ceramic half-cells of 50 × 50 mm^2 and 100 × 100 mm^2 with the sufficiently dense and gas-tight electrolyte layer were obtained. The cross-sectional

scanning electron micrograph (SEM) of the sintered half-cell before reduction is presented in Figure 5a. Lastly, a BCFZY cathode slurry was screen-printed onto the SZCY electrolyte and sintered at 900 °C for 2 h. After sintering, the cathode exhibited porous microstructure with a thickness of about 50 μm, as can be seen in the cross- sectional view of the cell (Figure 5b). The thicknesses of the electrolyte film and the supporting anode were approximately 16 μm and 400 μm, respectively. The electrochemical testing of the 50 × 50 mm^2 cell revealed the open circuit voltage (OCV) of about 1.18 V and the power density of 170 mW cm^{-2} under the supply of humidified hydrogen (5% H2O) to the anode and air to the cathode at 600 °C. The high OCV value confirmed the good gas-tightness of the electrolyte film. According to the authors, the obtained moderate power density can be improved by reducing the electrolyte thickness and enhancing the cathode microstructure. Nonetheless, this research demonstrates that sequential tape-casting combined with screen-printing is applicable for low-cost fabrication of the planar anode-supported SOFCs.

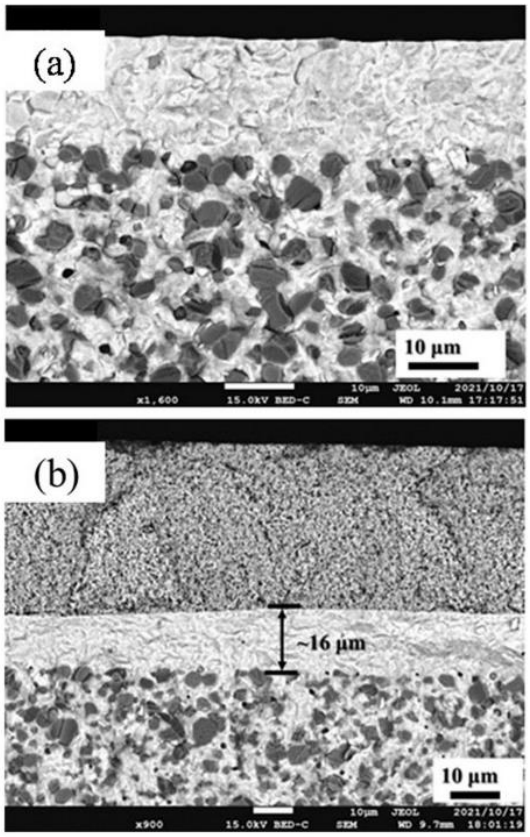

Figure 5 Cross-sectional SEM images of (a) sintered half-cell before reduction and (b) complete cell, with SZCY electrolyte deposited by tape-casting [95].

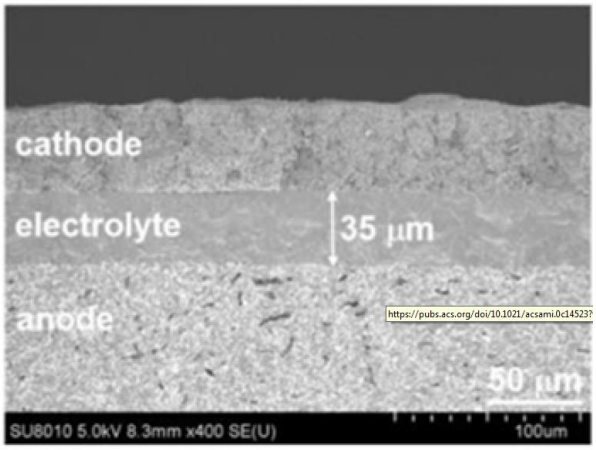

Figure 6 Cross-sectional SEM image of the sintered anode-supported cell with BCZY electrolyte deposited by dip-coating [96].

Liu et al. [96] reported another ceramic powder-based technology of manufacturing the planar anode-supported SOFCs with a proton-conducting electrolyte. A cermet of NiO–Ba0.96(Ce0.66Zr0.1Ni0.04Y0.2)O3-δ (BCZNY) was selected as the supporting anode. The powder mixture of NiO and BCZNY (weight ratio of 3:2) was axially pressed into button pellets and sintered at 800 °C for 2 h to obtain green anode substrates. For the electrolyte layer casting, a suspension containing the ceramic powder of proton electrolyte Ba(Ce0.7Zr0.1Y0.2)O3-δ (BCZY) was prepared. A thin electrolyte layer was deposited on the green substrates by dip-coating, and the obtained green half-cells were co-fired at 1400 °C for 5 h. Then a composite cathode layer consisting of La0.6Sr0.4Co0.2Fe0.8O3-δ (LSCF) and BCZY (weight ratio of 7:3) was brush-painted onto the central part of the electrolyte and sintered at 1000 °C for 2 h. The cross-sectional SEM image of the sintered cell is presented in Figure 6. As can be seen, the thickness of the electrolyte layer was approximately 35 μm. It was revealed that the addition of a small amount of Fe and/or Ni into BCZY improved the electrolyte conductivity and the SOFC performance at reduced temperatures. The doping was shown to enhance the electrolyte sinterability: the addition of 2 mol % of Ni/Fe helped fully densify the electrolyte by sintering it at 1400 °C. The highest electrochemical performance with a peak power density of 973 mW cm^{-2} at 700 °C was demonstrated by the fuel cell with the 2 mol% NiFe-doped BCZY electrolyte. Furthermore, it was shown that the ohmic resistance dominated the overall resistance of the fuel cell with the 35 μm thick electrolyte at 700 °C. Accordingly, reducing the electrolyte thickness is expected to result in a higher

peak power density; however, the cells with 20 μm and 10 μm-thick electrolyte layers demonstrated the similar values of the peak power densities (1070 and 1084 mW cm^{-2} at 700 °C, respectively), which indicated that the electrode performance also needed improvement.

Another important finding of this research is that diffusional interaction occurs between the electrolyte and cathode materials during the cell fabrication and operation [96]. Results of the energy-dispersive X-ray spectrometry (EDX) of the fuel cell after 200 h operation revealed the counter diffusion of Sr and Ba. Ba was found to have almost the same concentration in the cathode layer as in the electrolyte, while accumulation of Sr, Zr, and Y in the electrolyte indicated formation of the related oxides. The diffusion might cause the degradation of the cell performance. The problem can be solved by putting a barrier layer between the cathode and electrolyte layers and preventing the diffusion, or by using the cathode and electrolyte materials with a similar composition.

Le et al. reported a successful fabrication of the single proton-conducting planar SOFCs, which consisted of the supporting Nickel-electrolyte anode, $BaCe_{0.2}Zr_{0.6}Y_{0.2}O_{3-\delta}$ or $BaCe_{0.4}Zr_{0.4}Y_{0.1}Yb_{0.1}O_{3-\delta}$ electrolyte, and $BaCo_{0.4}Fe_{0.4}Zr_{0.1}Y_{0.1}O_3$ (BCFZY) cathode [97]. The anode supports were prepared by dry pressing the anode powder. The electrolyte layer was applied onto the supports by dip-coating of the suspension containing the powders of $BaCO_3$, CeO_2, ZrO_2, and Y_2O_3 in stoichiometric ratios. The obtained half-cells were sintered at temperatures between 1450 and 1550 ◦C for 15 h. Then the BCFZY cathode was brush-painted onto the electrolyte. The completed cells were sintered at 900 ◦C in air for 5 h. The single cells were approximately 1 mm thick and 38 mm in diameter, with an active area of about 5 cm^2. The thicknesses of the anode support, electrolyte and cathode layers were 1 mm, 20 μm and 20 μm, respectively. A small stack consisting of three single cells was assembled and tested in the fuel cell regime for 2500 h. The stack exhibited good electrochemical performance, with a maximum power density of 690 mW cm^{-2} upon supplying hydrogen to the anode and air to the cathode at 600 °C. The long-term testing of the stack revealed a voltage-degradation rate of 1.5% kh^{-1} at 550 °C, which is certainly a good result.

Majhi et al. successfully used the electrophoretic deposition technique for fabrication of a planar SOFC with a NiO–YSZ supporting electrode [98]. The 10 μm thick YSZ film deposited from 1 wt % suspension in acetylacetone at 50 V for 180 s and sintered at 1450 °C for 5 h exhibited dense grain morphology without cracks or pinholes. The obtained YSZ/NiO–YSZ bi-layers were co-sintered at 1450 °C for 5 h. An LSM–YSZ (LSM denotes $La_{0.8}Sr_{0.2}MnO_{3-\delta}$) cathode was paint brushed on the electrolyte layer and sintered at 1200 °C for 2 h. Testing of the completed SOFC in hydrogen as fuel and ambient air as oxidant exhibited a high OCV value of 1.03 V, which indicated satisfactory gas-tightness of the cell and peak power density of about 624 mW cm^{-2} at 800 °C. Impedance measurements revealed that the cell performance was restricted by the polarization losses, which can be reduced through optimization of the electrode microstructure.

Russian research group reported on fabrication process and testing of the planar large-area (100 × 100 mm^2) anode-supported cells with an oxide-ion conducting electrolyte based on zirconia and a bilayer Nickel-cermet supporting anode, using both the powder technologies (tape-casting and screen-printing) and physical vapor deposition (PVD) methods (magnetron sputtering and ion-beam treatment) [99]. Anode substrates consisting of $(Sc_2O_3)_{0.1}$–$(Y_2O_3)_{0.01}$–$(ZrO_2)_{0.89}$ (10Sc1YSZ) and NiO were fabricated by tape casting. To reach the target thickness of the supporting anode, five green tapes were laminated, four of which contained rice starch as pore former to create a highly porous layer, and the fifth tape had no pore former to make a denser thin functional layer on the top of the supporting anode. The laminated plates were sintered in air at 1350 °C for 2–4 h. Then, the two-layer electrolyte was deposited on the sintered supports by reactive pulsed dual magnetron sputtering in Ar/O_2 atmosphere: first, the layer of Zr–Y (85:15 at. %), and then the Ce–Gd (90:10 at. %) layer were deposited. The substrates were heated to 400 °C to enhance the film density. To improve the film gas-tightness, the surface of the deposited electrolyte was treated with ion beams for 10 min, which allowed it to heat and densify the upper electrolyte layer, avoiding unwanted chemical interaction between the electrolyte and anode materials. This method of enhancing the gas-tightness of refractory solid oxide films deposited by sputtering techniques was shown to be effective in [102]. A cross-sectional SEM image of the fabricated anode-supported half-cell is presented in Figure 7. The total thickness of the sputtered two-layer electrolyte was about 5.5 μm, which

is much less than a typical thickness of layers deposited by the ceramic powder-based technologies (tens micrometers). To complete the cell, the La0.8Sr0.2CoO3-δ cathode layer was applied by screen-printing. The fuel cell demonstrated an excellent electrochemical performance: the peak power densities of 1.8 W cm^{-2} and 0.96 W cm^{-2} at 800 and 700 °C were attained. The decrease in power density by half upon lowering the operating temperature to 700 °C was caused by an increase in the polarization resistance by more than 5 times, whereas the contribution of ohmic losses changed insignificantly. Thus, further optimization of the composition and microstructure of the electrodes is needed. The long-term stability of the fabricated cells was not reported. Nonetheless, this study showed that the applied combination of the powder and vacuum deposition techniques for the solid-oxide cells manufacturing has prospects for a scalable production.

Combination of the powder and PVD techniques for fabrication of the planar anode-supported SOFCs was also used by Kang et al. [100]. The supporting NiO–YSZ electrode (weight ratio of NiO to YSZ of 63:37) consisted of two layers – a highly porous anode collector layer (ACL) and a denser thin anode functional layer (AFL) – as well as in the cell described in [99]. The ACL was made by tape casting using carbon black and graphite as pore formers (10 wt%). The tapes were dried at room temperature and atmospheric pressure for 48 h, then cut and pre-sintered at 1000 °C for 4 h. The AFL was prepared by the spin-coating technique with the NiO–YSZ paste mixture (weight ratio of NiO to YSZ of 47:53). The bilayer supports, co-sintered at 1350 °C for 4 h, were approximately 2.5 cm in diameter and 500 μm in thickness. Then, a bilayer electrolyte was deposited: first, 1 μm-thick YSZ thin film was deposited on the anode substrate by direct current reactive sputtering in Ar-O2 (8:2) at room temperature; then, 300 nm Ce0.9Gd0.1O2-δ (GDC) thin film was deposited by radio-frequency sputtering in the same atmosphere. After the electrolyte deposition, the half-cells were co-sintered at 1000 °C for 1 h. La0.6Sr0.4Co0.2Fe0.8O3-δ (LSCF)–GDC (weight ratio of 6:4) cathode layer was coated by screen-printing and sintered at 970 °C for 2 h. SEM study showed that the thickness of the sintered cathode layer was about 30 μm; the ~1.3 μm thick electrolyte had dense fine-grained morphology without pinholes or cracks, with grain size up to 100 nm. The fabricated SOFC demonstrated the peak power density of about 600 mW cm^{-2} at 650 °C.

Fabrication of a thin film electrolyte using PVD technology for the planar type 10 × 5 cm^2 solid oxide fuel cells was reported by Solovyev et al. [101]. A commercially available NiO–YSZ anode (SOFCMAN, China) with a thickness of 400 μm was used as a substrate. The 4 μm thick YSZ and 2 μm-thick GDC electrolyte layers were deposited by reactive magnetron sputtering using metallic targets Zr0.86Y0.14 and Ce0.9Gd0.1 in Ar–O2 gas mixture at the substrate temperature of 450 °C. The deposited films were sintered at 1200 °C for 1 h in air. Then, a composite cathode La0.6Sr0.4Co0.2Fe0.8O3–Ce0.9Gd0.1O3 (LSCF–GDC) was screen-printed on the electrolyte surface and dried at 100 °C for 1 h. The sintering of the cathode layer was completed during the first testing of the cell at 750°C. After sintering, the cathode thickness was 15 μm. No cracks or delamination of the layers were found. Testing of the fuel cell demonstrated a high OCV of 1.14 V at 750 °C, which confirmed the sufficient gas-tightness of the electrolyte layer. However, the peak power density of the cell was rather low, approximately 470 mW cm^{-2}. The authors explained it by the high resistance of the cathode/current collector interface (the latter was made of stainless steel) due to insufficiently tight contact over the large interface area. Nonetheless, the possibility of using PVD technology for manufacturing the large-area planar type SOFCs with a thin film electrolyte was demonstrated. Moreover, a three-cell SOFC stack was assembled using the 10 × 5 cm^2 anode-supported cells, metallic interconnects, and glass sealing. The peak power density of the stack (520 mW cm^{-2} at 750 °C) was just slightly higher than that of the single cell, which may indicate problems with the stack assembling.

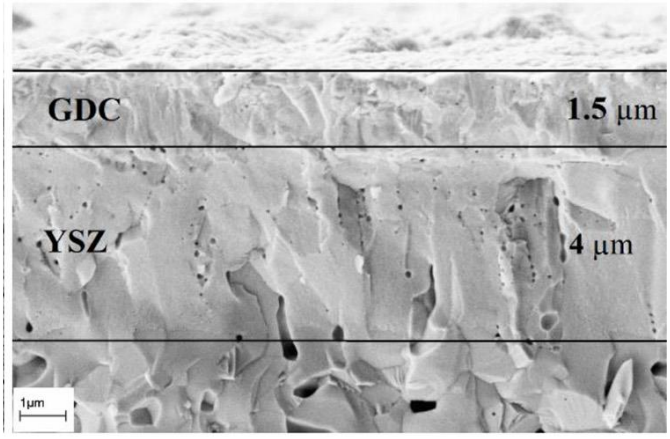

Figure 7 Cross-sectional SEM image of the anode-supported half-cell with YSZ/GDC electrolyte deposited by reactive pulsed dual magnetron sputtering [99].

Attempts to increase an effective area of the planar thin film SOFCs often cause serious cell integrity problems. Kim et al. [103] investigated the thermal and structural stability of a planar anode-supported SOFC using a 10 × 10 cm^2 single cell and found that the cell was vulnerable to the thermal RedOx cycling caused by poor sealing. It was concluded that the cell gas tightness had to be enhanced to increase the lifespan. Moreover, thermal stresses caused by mismatch of thermal expansion between cell components and thermal gradients, which were shown to be significant in the planar SOFCs, can lead to microstructural changes, fractures, and delamination [104-106].

Thus, the current state of research confirms that the planar anode-supported SOFCs have a potential of highly efficient electricity generation, but serious challenges, mainly related to the stack assembling and the long-term stability, need to be addressed [101,103,107]. The low-cost, simple, and scalable ceramic powder-based technologies are applicable for deposition of a gas-tight electrolyte layer with a thickness of tens micrometers. To obtain thinner membranes, it is more appropriate to use PVD or CVD technologies.

4.2 Microtubular anode-supported SOFCs

The possibility of manufacturing microtubular SOFCs was first reported at the end of the 20th century: Alston et al. [108] demonstrated extrusion of thin YSZ ceramic tubes with wall thickness of 100–200 μm, which could be used as the electrolyte for SOFC operation, and assembled a stack of 1000 microtubular cells. It was shown that the tubular fuel cells could withstand 200 °C/min temperature rise. The peak power density of the reactor was not high – only 82 mW cm^{-2} at 850°C; nonetheless, significant advantages of the microtubular SOFCs, such as small size and fast start-up, were demonstrated. Later, it was reported that even faster thermal cycling did not cause any degradation of the microtubular cells: the stacks could withstand the heating rates of 550 °C min^{-1}, producing normal power at the operating temperature of 800 °C [109]. The single cells were put into preheated ovens for heating up and pulled out for cooling down. Fast start-up and small size are essential for use as auxiliary power units on a vehicle, automotive power supply systems, mobile electricity generators, and battery rechargers.

Currently, the most studied microtubular cells are the anode-supported ones, as this configuration allows for the reduction of the ohmic losses [39,110–112,117–119]. The supporting microtubes are usually made by phase inversion method, which has the flexibility in control and tailoring of the microstructure. Monzón et al. [110] reported on fabrication of NiO–YSZ (volume ratio of 1:1) tubular anode supports by the phase inversion process. YSZ electrolyte film was deposited on the NiO–YSZ tubes by dip-coating and co-sintered at 1500 °C for 2 h. Then, a multilayer cathode $(La_{0.8}Sr_{0.2})_{0.98}MnO_3$ (LSM) was deposited by dip-coating as follows: first, a composite of LSM–YSZ (weight ratio of 1:1) was deposited on the electrolyte surface to serve as a functional layer, then the composite with a higher LSM content (weight ratio of 4:1) was applied to the current collector layer. The fabricated microtubular cells were 6 mm in length, 3.2 mm outer diameter, 2 mm inner diameter, 20 μm YSZ electrolyte, 15 μm LSM–YSZ functional layer and 15 μm LSM–YSZ current collection layer. The cell was tested using H_2–3% H_2O as a fuel at 800 °C for a period over 1000 h. High OCV value (~1.1 V) proved the good gas-tightness of the cell. Cross-sectional SEM images of the fabricated microtubular anode-supported cell before and after 1000 h operation, shown in Figure 8, demonstrate that nickel coarsening

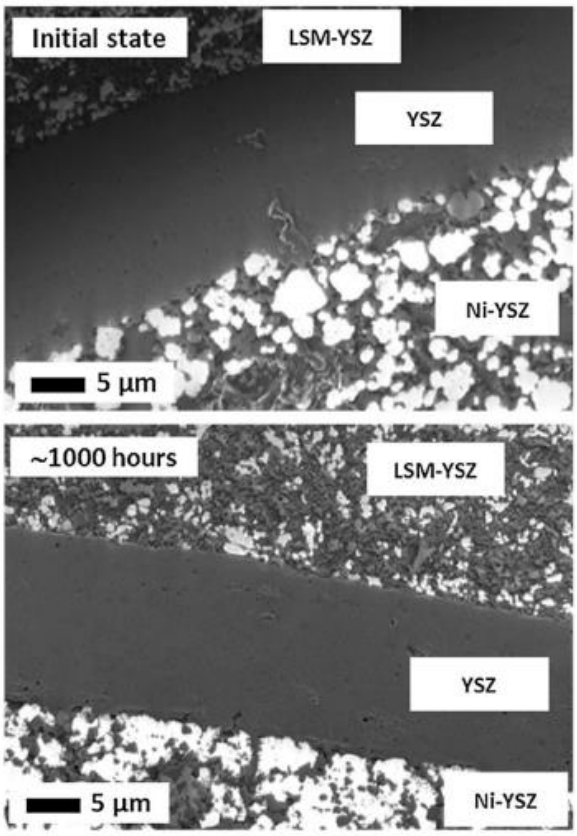

Figure 8 Cross-sectional SEM images of microtubular anode-supported cell with dip-coated YSZ electrolyte before and after 1000 h operation [110].

occurs during the long-term operation; however, impedance measurements revealed negligible cell degradation. Chronoamperometric testing of the cell performed at 800 °C, 0.8 V and 5 cm^3 min^{-1} of humidified hydrogen (3% H2O) as fuel demonstrated almost constant current densities of ~400 mA cm^{-2} for 1000 h.

The microtubular type electrochemical cells are also being developed in Russia: the use of the phase inversion process for fabrication of the anode-supported fuel cells and the oxygen permeable membranes was reported in [111,121-123]. Zazhigalov et al. [111] reported on manufacturing the microtubular anode supports NiO–YSZ using the polymer paste made of the stoichiometric amounts of YSZ and NiO powders, N-methylpyrrolidone as a solvent, and polysulfone as a polymer (weight ratio of 12:4:1). The polymer paste was extruded in the coagulation bath. The obtained green tubes were calcined at 600 °C for 2 h to burnout the organic binder and sintered at 1150 °C for 6 h in air. A 10 μm layer of YSZ electrolyte and a 20 μm layer of composite cathode La0.6Sr0.4Co0.2Fe0.8O3-δ(LSCF)–Ce0.9Gd0.1O2-δ (GDC) (weight ratio of 1:1) were deposited by dip-coating. Electrochemical testing of the microtubular fuel cell demonstrated high current density of about 200 mA cm^{-2} at 800 °C.

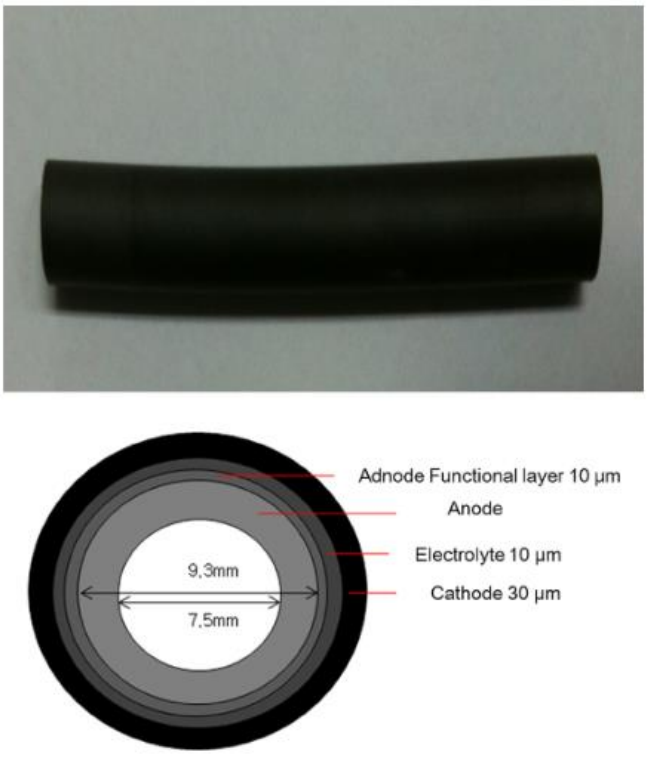

Figure 9 Cell configuration of tubular Ni–BZCY-supported SOFC developed in [112].

A microtubular SOFC with the proton-conducting Ba(Zr0.1Ce0.7Y0.2)O3-δ (BZCY) electrolyte was developed by Min et al. [112]. Ni–BZCY anode tubes were fabricated by the phase inversion method and served as the cell support. The green tubes were dried for 2–3 days and pre-sintered at 1100 °C for 3 h. The inner and outer diameters of the anode tubes were about 7.5 mm and 9.3 mm, respectively, and the length reached 4 cm (see Figure 9). Then, Ni–BZCY nanocomposite slurry was deposited on the tubes by dip-coating to act as an anode functional layer. Later, the layer of BZCY electrolyte was deposited by vacuum slurry coating method and co-sintered at 1450 °C for 5 h. Finally, LSCF–BZCY cathode (LSCF denotes La0.6Sr0.4Co0.2Fe0.8O3-δ) was prepared by dip-coating, and the completed cell was sintered at 1100 °C for 3 h. The fabricated tubular-type cell exhibited good performance: the OCV value of 1.01 V and the peak power density of about 0.5 W cm^{-2} were measured upon supply of humidified hydrogen (5% H2O) as fuel at 700 °C.

It is well known that microstructure of a supporting anode has a strong effect on the SOFC performance. A significant advantage of the porous supporting electrodes produced by the phase inversion method is that the pore orientation and size facilitate diffusion of gaseous fuel to the triple phase boundary where the electrochemical reactions occur, which should enhance the SOFC performance [87,111]. For illustration, the cross-sectional SEM images of the YSZ film deposited by dip-coating on the NiO–YSZ tube produced by phase inversion are presented in Figure 10.

Rabuni et al. [114] developed an enhanced tubular electrode design with the help of a modified phase-inversion method. YSZ microtubes were produced by extrusion of a suspension containing YSZ ceramic powder through a custom-designed spinneret into an external coagulation bath of deionized water. The green microtubes were left in water overnight to complete the phase inversion and then sintered at 1450 °C for 6 h. SEM images of the fabricated YSZ tube presented in Figure 11 demonstrate a non-uniform structure consisting of a thick porous layer with radially oriented microchannels and a dense thin outer layer with a thickness of about 10 μm. The dense layer serves as an electrolyte, while the porous layer is an appropriate framework for deposition of anode materials. The dual-layer cathode consisting of an inner LSM–YSZ (weight ratio of 1:1) layer and an outer LSM layer was painted onto the YSZ microtubes and sintered at 1000 °C for 2 h. The Cu–CeO2 anode was

deposited onto the inner surface of the porous YSZ microtubes via vacuum-assisted co-impregnation process, using a mixed aqueous solution of copper nitrate and cerium nitrate; the impregnation was followed by heating to 450 °C (1 h) to decompose the nitrates. The impregnation process was repeated until a target loading of 25 wt% was achieved. Thus, a continuous and well-dispersed Cu-CeO2 layer was incorporated inside the porous framework of the supporting layer. The open microchannels should facilitate the gas transport to the triple phase boundary, and, consequently, the SOFC performance due to a lower concentration polarization.

Electrochemical performance of the fabricated cells was tested in dry H2 or CH4 as fuel and ambient air as oxidant. The OCV value of up to 1.19 V for H2 at 650 and 700 °C indicated high gas-tightness of the YSZ membrane. The peak power density of up to 0.4 W cm^{-2} and 0.55 W cm^{-2} was achieved at 700 and 750 °C with H2 as a fuel. High performance of the SOFC may be attributed to the unique hierarchical structure of the supporting microtubes.

Majewski et al. studied the possibility of using silver as a cathode material, an interconnect wire, and a sealing for anode lead connection in microtubular SOFCs [115]. Though the addition of silver as a cathode conductive layer reduced the cell overpotential and increased the cell performance, it was revealed that silver may lead to the cell degradation, since it is unstable in the interconnect and cathode environments. Moreover, silver may migrate from a cathode to electrolyte surface at the SOFC operating temperatures, leading to a short circuit formation.

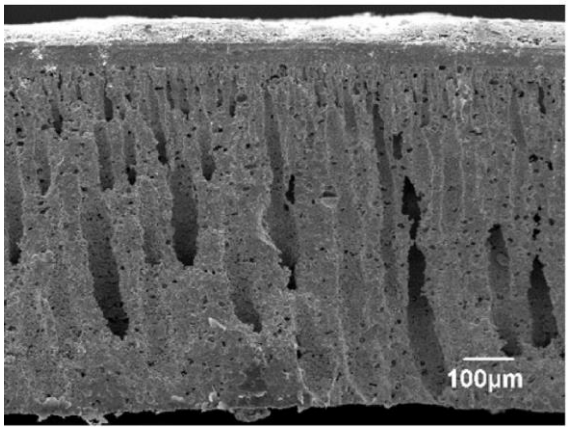

Figure 10 Cross-sectional SEM images of YSZ film deposited on NiO-YSZ cermet produced by phase inversion [87].

Villegas et al. [116] reported on fabrication and testing of microtubular SOFCs fabricated by dip coating of electrolytic (Ce0.8Gd0.2O1.95), anodic (50 wt% NiO–50 wt% Ce0.8Gd0.2O1.95), and cathodic (La0.8Sr0.2Co0.2Fe0.8O3) suspensions onto the polymethylmethacrylate cylindrical rods which were used as sacrificial cores. The fabricated cell had a length of ~2 cm, an outer diameter of ~1.5 mm; the anode, electrolyte and cathode thicknesses were ~350, 15 and 40 µm, respectively. The fuel cell testing, which was performed in air and hydrogen humidified at room temperature at 500 °C, revealed good electrochemical characteristics: the OCV value reached about 1 V, the peak power density reached ~300 mW cm^{-2}. However, the single microtubular cell cracked during the testing, and the cell characteristics significantly dropped, which indicated that chemical, thermal and mechanical engineering issues still remained unresolved.

Anode-supported microtubular SOFCs with a diffusion barrier layer to mitigate the interaction of YSZ electrolyte and La0.6Sr0.4Co0.2Fe0.8O3-δ (LSCF) cathode, which exhibited excellent performance, were prepared by Milcarek et al. [117] using the extrusion, dip-coating and wet powder spray techniques. YSZ electrolyte with a thickness of 22 µm was dip coated onto the extruded NiO–YSZ tubes and sintered at 1400 °C for 4 h. Then a buffer layer of Sm0.2Ce0.8O2-δ (SDC) or Gd0.1Ce0.9O1.95 (GDC) was deposited by spraying and sintered at 1350 °C for 4 h. To complete the cell, the cathode layer of LSCF–SDC (weight ratio of 7:3) and LSCF–GDC (weight ratio of 7:3) was dip coated and sintered at 1100 °C for 2 h. The best electrochemical performance was demonstrated by the cell with the 1.7 µm thick SDC buffer layer deposited by 105-step spraying: the OCV value reached more than 1.1 V, and the peak power density was about 1 W cm^{-2} upon supply of hydrogen as a fuel and air as an oxidant at 750 °C. The thinner SDC and GDC layers resulted in high polarization and ohmic resistance, which was caused by interdiffusion of the cathode and electrolyte materials, resulting in the formation of non-conductive layers. Furthermore, it was shown that GDC was less effective as a barrier layer preventing species interdiffusion than SDC. Milcarek et al. reported the highest cell performance for the micro- tubular SOFCs to date. However, long-term testing of the cell was not reported.

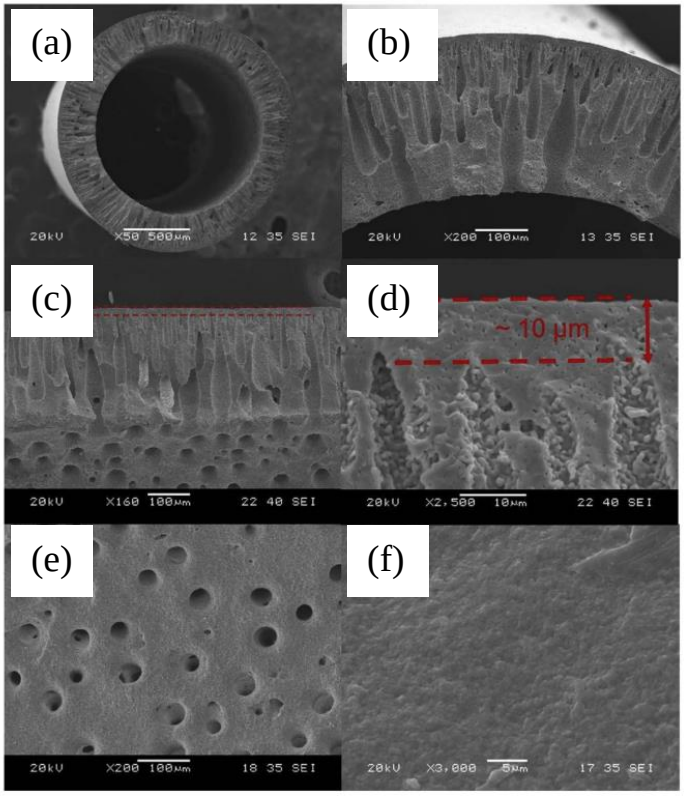

Figure 11 SEM images of the sintered YSZ microtube: (a–d) cross-sectional images, (e) inner surface, (f) outer surface [114].

Excellent power generation performance of the microtubular solid oxide cell operating in both the SOFC mode and the solid oxide electrolysis cell (SOEC) mode was reported by Sahu et al. [118]. The cell was fabricated by the multi-step dip-coating technique using Ni–YSZ, Ni–ScSZ (ScSZ denotes scandia stabilized zirconia), ScSZ, Sm-doped CeO2 (SDC) and LSCF to form the supporting fuel electrode layer, the fuel electrode functional layer, the electrolyte layer, the diffusion barrier layer, and the air electrode, respectively. Each dip-coating step was followed by drying in air. The thicknesses of the Ni–YSZ, Ni–ScSZ, ScSZ, SDC, and LSCF layers in the fabricated cell were 400 μm, 15 μm, 10 μm, 2 μm, and 20 μm, respectively. Electrochemical performance of the fabricated cells was tested in dry hydrogen as fuel and ambient air as oxidant. The OCV value was above 1.2 V in the temperature range of 700–800 °C, which proved the excellent gas-tightness of the cell. The peak power density reached 0.69 W cm^{-2} at 800 °C. Testing of the cell under reversible operation for more than 500 h revealed that the degradation rate was much higher in the electrolysis mode (~50%) than in the fuel cell mode (~31%). Analysis of the impedance data and the scanning electron microscopy images of the cell after the long-term operation led to the conclusion that the coarsening of the Ni particles of the fuel electrode and the formation of zirconia and NiO nanoparticles at the electrode/electrolyte interface during the electrolysis operation were the main reasons for the degradation.

The long-term stability study of the anode-supported microtubular SOFCs was conducted by Laguna-Bercero et al. [119]. The cells were fabricated using the YSZ–NiO supporting tubes prepared by the cold isostatic pressing and pre-sintering at 1000 °C. The YSZ electrolyte layer was deposited onto the supporting tubes by spraying, and the half-cells were co-sintered at 1350 °C for 2 h. The bilayer cathode was applied by dip-coating using the $(La_{0.8}Sr_{0.2})_{0.98}MnO_3$ (LSM) powder. First, the LSM–YSZ composite with the weight ratio of 1:1 was deposited as a functional layer, then the composite with the weight ratio of 4:1 was applied as a current collector layer. After sintering, the electrolyte thickness was 15 μm, and the total thickness of the cathode was about 40 μm. The tubular cell had 100 mm length, 2.4 mm inner diameter, and 340 μm total thickness. The fabricated cell was tested under current load for 650 h at 766–873 °C. The degradation rate was about 4% per 1000 h. The cells demonstrated an excellent resistance to rapid thermal cycling; however, the cracking of the electrolyte layer was observed after the reoxidation, which indicated insufficient redox stability of the cell.

4.3 Dense hydrogen permeable metal anode-supported SOFCs

Exceptionally high electrical generation performance was reported for the SOFCs with a thin proton-conducting ceramic electrolyte supported on a dense hydrogen permeable metal anode [124-126]. Ito et al. reported on fabrication of an ultra-thin $SrZr_{0.8}In_{0.2}O_{3-\delta}$ electrolyte on an 80 μm thick Pd foil by pulsed laser deposition [124]. Thickness of the electrolyte films was varied from 0.7 to 6.0 μm by controlling the deposition time. To complete the cell, a 30 μm thick $La_{0.6}Sr_{0.4}CoO_{3-\delta}$ cathode was screen-printed onto the electrolyte film and dried with a heat gun. The highest OCV values (about 1.1 V at 400 °C under hydrogen and air supply to the anode and the cathode) were obtained for the electrolyte film thicknesses of 4.0 and 6.0 μm, while OCV values for the thinner films (0.7 μm and 2.0 μm) were approximately 1 V, which indicated that the film gas-tightness increased with a rise of thickness. Nevertheless, the cells with the thinner electrolytes demonstrated the higher performance. Analysis of the

polarization losses based on the impedance measurements revealed that the cathode polarization dominated over other losses for the fuel cells with the thinner electrolytes, while the increase of electrolyte thickness to 6.0 μm caused the prevalence of the ohmic losses. The anode polarization was the lowest for all fabricated cells.

A hydrogen membrane-supported SOFC consisting of a Pd solid anode, 1 μm thick $BaCe_{0.8}Y_{0.2}O_{3-\delta}$ electrolyte, and $La_{0.6}Sr_{0.4}Co_{0.2}Fe_{0.8}O_{3-\delta}$ cathode was fabricated and tested by Aoki et al. [125]. The electrolyte film was deposited by RF sputtering on a 0.5 mm thick Pd foil. A porous cathode was deposited by screen-printing and heated with a heat gun for 2 min. Despite the fact that proton conductivity of the electrolyte films was 2 orders of magnitude smaller than the values reported for the bulk samples, the fabricated SOFCs provided the OCV values of 1.08 V and an extremely high power density of 1.05 W cm^{-2} at 600 °C under the supply of hydrogen to the anode and wet air to the cathode.

Application of a PdAg alloy as a hydrogen permeable supporting anode, instead of expensive pure Pd, was reported by Aoki et al. [126]. 1 μm thick $BaCe_{0.8}Y_{0.2}O_{3-\delta}$ films were deposited on 0.03 mm thick $Pd_{1-x}Ag_x$ foils (x = 0, 0.2, 0.4) by RF sputtering. The cathode was prepared as described in [124]. The fabricated cells were tested in dry H_2 supplied to the Pd anode side and wet O_2/Ar mixed gas (pH_2O = 3 kPa) fed to the cathode side. It was revealed that the hydrogen permeability of the supporting anodes was crucial to the cell performance. The cell with the $Pd_{0.8}Ag_{0.2}$ anode possessing high hydrogen permeability displayed low anode overpotentials when operated at high current densities of about 1 A cm^{-2}. On the other hand, large concentration overpotentials were observed for the cells with the $Pd_{0.6}Ag_{0.4}$ anodes, which showed relatively low hydrogen permeability. The $Pd_{0.8}Ag_{0.2}$-supported fuel cell exhibited a superior performance with the peak power density reaching 1.2 W cm^{-2} at 600◦C.

The reported results for the dense hydrogen permeable metal anode-supported SOFCs demonstrate their superior electrical generation performance due to the unique transport properties of Pd or Pd-containing alloys. However, high thermal expansion mismatch between ceramic and metal components might affect the thermal cycling ability of these SOFCs; furthermore, diffusional interaction can lead to degradation of the cell components. Thus, the long-term testing and degradation study of this type of SOFCs, which have not been reported, are strongly required.

5. Metal-supported SOFCs

Development of thin film SOFCs with an external metal support also attracts extensive attention from researchers. In this type of cells, both the ohmic and polarization resistances can be minimized due to the possibility of decreasing the thicknesses of all functional layers by depositing them on a metal support, which provides mechanical strength, high electrical and thermal conduction. The metal support is typically made from inexpensive and robust porous material by using powder metallurgy, laser drilling, or tape-casting technologies [127,128]. The metal-supported SOFCs are characterized by faster start-up times, superior mechanical stability and thermal cyclability compared to all-ceramic SOFCs [127-133]. Furthermore, manufacturing costs of the metal-supported SOFCs are lower due to the less-expensive metal substrate. The supporting metal is required to possess similar thermal expansion to that of the electrolyte to enable fast thermal cycling. A variety of metals and alloys, including Ni [134,135], Ni-Fe [136], Ni-Al [137], ferritic stainless steel [130,132], and others [127,129,133] were reported to be used as the supports.

Application of porous pure Ni as a support material was reported by Hwang et al [134]. SOFCs were fabricated by atmospheric plasma spraying of YSZ/NiO anode, $La_{0.8}Sr_{0.2}Ga_{0.8}Mg_{0.2}O_{3-\delta}$ (LSGM) electrolyte and $La_{0.58}Sr_{0.4}Co_{0.2}Fe_{0.8}O_{3-\delta}$ (LSCF) cathode on porous Ni substrates. SEM study of the polished cross-section of the fabricated YSZ/Ni–LSGM–LSCF cell after the thermal treatment at 1000 °C for 2 h and the OCV testing for 55 h showed that the layers exhibited good adhesion without cracks or delamination; the thicknesses of LSCF, LSGM and YSZ/Ni layers reached 20–30, 50–60 and 10–20 μm, respectively. Analysis of the impedance data of the cells sintered at different temperatures in the range of 820–1150 °C (2 h) revealed that the cell sintered at 1000 °C had minimum resistance. This cell showed high OCV value (above 1 V), indicating the good gas-tightness of the electrolyte, and the peak power densities of 440 mW cm^{-2} at 800 °C and ~170 mW cm^{-2} at 700 °C. Element interdiffusion between YSZ/Ni anode and LSGM electrolyte was observed at higher sintering temperatures. The interdiffusion could lead to generation of high resistive phases and, consequently, to degradation of the SOFC performance.

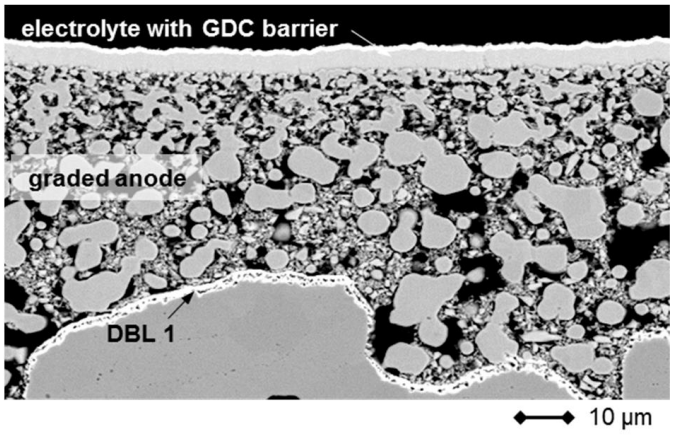

Figure 12 Cross-sectional SEM-images of the metal-supported half-cell with the graded Ni-YSZ anode, sputtered YSZ electrolyte and GDC diffusion barrier layers (DBL) [130].

Manufacturing of a metal-supported SOFC based on a porous steel substrate, a graded three-layer Ni/YSZ anode, and a thin YSZ membrane was described in [130]. First, the 0.8 mm thick porous (porosity of about 40%) supports based on FeCr alloy (Cr26-Fe) were fabricated by the powder-metallurgical process. The fabricated substrates were coated with a 500 nm thin gadolinium doped ceria (GDC) layer by magnetron sputtering to avoid diffusion of Fe and Cr into the anode. It is known that Fe and Cr form alloys with the Ni-catalyst, which results in degradation of SOFC performance [131]. Then, a graded Ni/YSZ anode with a thickness of 40 µm was applied to the substrate by 3-step screen-printing, followed by annealing at 1180 °C in the H_2 atmosphere (to avoid oxidation of Ni). In each screen-printing step, the ink composition was varied to gradually decrease the porosity and the particle size in the anode layer. After the anode deposition, YSZ electrolyte layer with a thickness of 4 µm was applied by gas-flow sputtering. A 500 nm thin GDC layer was deposited by magnetron sputtering over the YSZ layer to serve as a diffusion barrier. Finally, a 40 µm LSCF cathode was screen-printed on top of the magnetron-sputtered GDC. The cross-sectional SEM-images of the metal-supported half-cell with the fabricated cell are given in Figure 12.

Testing of electrical performance of the fabricated single fuel cells with 1 cm^2 area cathodes revealed the power density of about 1 W cm^{-2} and the current density of 1.5 A cm^{-2} at 800 °C in air at the cathode and H_2 + 3% H_2O atmosphere at the anode. A stack of two single cells with 84 cm^2 active area exhibited the peak power density of about 430 mW cm^{-2} at 750 °C. However, degradation of the stack performance was higher compared to traditional all-ceramic SOFCs. It was revealed that progressive corrosion of the porous metal-support occurred which indicated the insufficient stability of the GDC barrier layer under the fuel cell conditions. The authors concluded that the lifetime of the metal-supported SOFC can be increased by applying a more redox-stable barrier layer.

Uchiyama et al. reported on manufacturing of a SOFC with a thin Y-doped $SrZrO_3$ electrolyte supported by a porous stainless-steel plate with a Pd layer [132]. The substrates were fabricated by sintering of stainless-steel powders. A several-µm thick Pd layer was deposited by plating on the polished surface of the sintered substrates. $SrZr_{0.8}Y_{0.2}O_{3-\delta}$ (SZY) films were deposited on the substrates by spin-coating. The solution with concentration of 5 wt% was repeatedly spin-coated on the substrates, until the film thickness reached about 300 nm. The deposited film was annealed at 500–800 °C for 1 h. Although the possibility of deposition of dense thin SZY films on the Pd-coated porous stainless-steel substrates was demonstrated, the authors noted that high temperature (> 1000 °C) sintering of the cathode layer caused deformation of the substrate.

Fabrication and testing of a micro-SOFC with a thin YSZ electrolyte supported by porous dual-layer stainless steel/composite was reported by Kim et al. [133]. The composite layer consisted of YSZ and La-doped $SrTiO_3$ (LST) due to the comparable thermal expansion to those of YSZ and stainless steel, as well as high electronic conductivity and redox stability. The dual-layer substrate was prepared using tape-casting and lamination, followed by co-firing in reducing gas to avoid oxidation of stainless-steel. The 40 µm thick LST-YSZ layer had pore size of ~500 nm and surface roughness of 44 nm. The layers of NiO-YSZ anode, YSZ electrolyte and $La_{0.7}Sr_{0.3}CoO_{3-\delta}$ (LSC) cathode were deposited by pulsed laser deposition (PLD). Finally, a Pt current collector was sputtered on top of the cathode. The cross-sectional SEM images of the fabricated layers are presented in Figure 13. The cell consisted of 0.7 µm thick LSC cathode, 2 µm thick YSZ electrolyte, and 0.6 µm thick Ni-YSZ anode. Both electrodes possessed porous morphology with the grain and pore size of < 100 nm. The YSZ layer was dense and uniform. Analysis of the mutual elemental diffusion between LST-YSZ and stainless-steel layers co-fired at 1250 °C revealed that diffusion of Fe or Cr from the stainless-steel layer was negligible, thus the LST-YSZ composite could be used as the diffusion barrier layer.

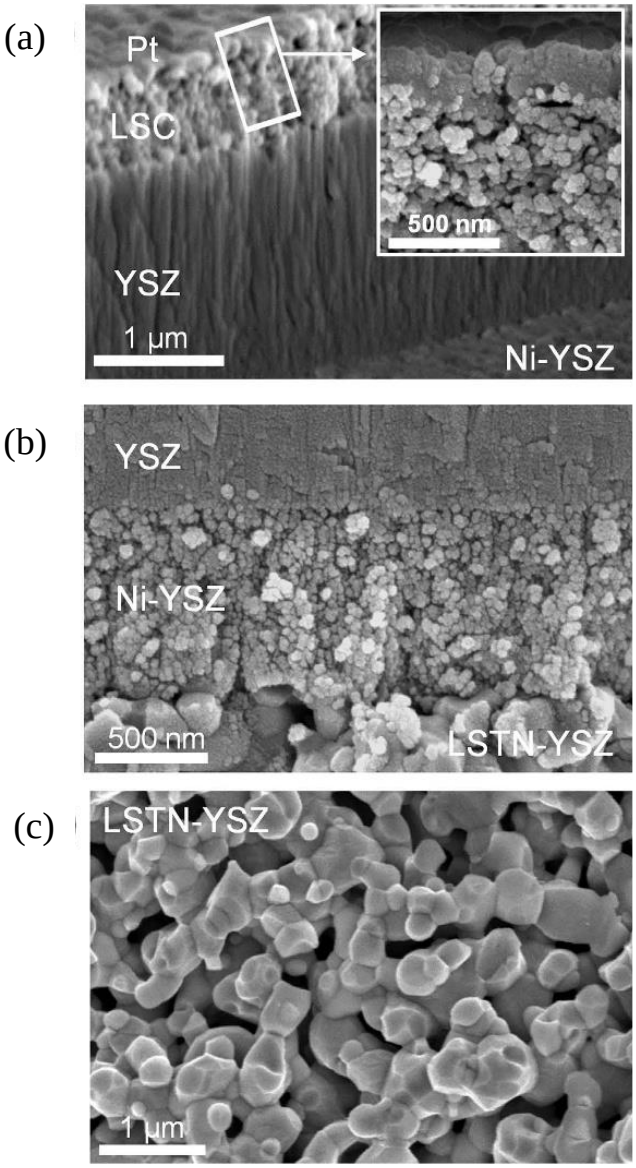

Figure 13 Cross-sectional SEM images of (a) Pt/LSC/YSZ/Ni-YSZ, (b) YSZ/Ni-YSZ/LST-YSZ, and (c) LST-YSZ layers [133].

The OCV value of the fabricated cell, measured at 450–550 °C under supply of air to the cathode and humidified hydrogen (3% H_2O) to the anode, was over 1.05 V. The high OCV value confirmed the high gas-tightness of the thin film electrolyte and good sealing of the cell. The peak power density reached 560 mW cm^{-2} at 550 °C and exhibited no degradation during rapid thermal cycling. Thus, the stainless steel/LST-YSZ composite supported cell has the potential of being used as a power source for portable electronic devices that require high power density and fast thermal cycling.

Ju et al. reported on fabrication of Ni-Fe metal supported fuel cell with LSGM ($LaGaO_3$ doped with strontium and magnesium) electrolyte, which was deposited by PLD, and $Sm_{0.5}Sr_{0.5}CoO_3$ cathode applied by slurry coating method [138]. LSGM electrolyte is known to possess high nearly pure ionic conductivity [138,139]; however, it easily reacts with Cr_2O_3 and Cr-containing vapors, which limits the use of stainless steel supports [140]. Moreover, it reacts with Ni in the anode or Ni–Fe metal support. The interaction with nickel can be suppressed by application of an additional thin layer of ceria-based electrolyte between the electrolyte and metal support. The fabricated cell demonstrated a high peak power density of 1.6 and 0.9 W cm^{-2} at 700 and 600 °C, respectively, in moist hydrogen as a fuel and oxygen as an oxidant. However, the power density decreased by about 50% upon the second cooling/heating cycle, which could be caused by the thermal cycling or oxidation of the support. Long-term testing of the cell was not reported.

Remarkable performance of stainless steel-supported SOFCs was reported by Dogdibegovic et al. [142]. Green cells were assembled by laminating the stainless-steel /10Sc1CeSZ/stainless-steel layers (10Sc1CeSZ denotes $(Sc_2O_3)_{0.1}$–$(CeO_2)_{0.01}$–$(ZrO_2)_{0.89}$ electrolyte), prepared by tape-casting. Cells were fired in air at 525 °C for 1 h to remove the binder and poreformer, then sintered at 1350 °C for 2 h in the Ar + 2% H_2 atmosphere. The prepared cells consisted of 7 μm or 12 μm thick electrolyte, 200 μm thick porous metal supports, 25 μm thick porous cathode and anode backbones. PrOx was selected as a cathode material, while Sm-doped ceria-40% Ni composite was chosen as an anode. The anode and cathode sides of the cell were infiltrated with corresponding metal nitrates. The fabricated cell with 7 μm thick electrolyte demonstrated the peak power density of 1.56 W cm^{-2} at 700 °C and 2.85 W cm^{-2} at 800 °C upon supply of air to the cathode and hydrogen, humidified at room temperature, to the anode. This is the highest cell performance reported for stainless steel supported SOFCs to date. However, the issues of diffusional interaction between the metal support and electrode materials were not considered and the long-term testing of the cell was not reported.

Pirou et al. fabricated a monolithic metal-supported fuel cell stack with high power density using cost-competitive and scalable manufacturing methods [143]. The configuration of a single cell included a 10 μm thick Sc-doped YSZ (ScYSZ) electrolyte, sandwiched between two porous 15 μm thick electrodes (ScYSZ-Fe22Cr composite). These electrode/electrolyte/electrode layers were placed

between the thicker layers consisting of gas distribution channels (250 μm) and metallic interconnects (dense Fe22Cr, 150 μm). All components of the monolith were fabricated by tape-casting, then the layers were laminated. The green monoliths were debinded at 600 °C for 4 h in air and then sintered at 1290 °C for 6 h in H2 in one firing step. The sintered cells were infiltrated with Gd-doped ceria to form a diffusion barrier layer, preventing diffusional interaction of electrodes with steel during operation. Electrochemical testing of the monolith heated to 780 °C upon feeding dry hydrogen to the anode and oxygen to the cathode showed the OCV value of 1.07 V and the peak power density of about 0.47 W cm^{-2}. The developed technology allows one to reduce the total number of firing steps in the manufacturing process.

Summarizing the findings in the area of the metal-supported SOFCs, we must acknowledge the current challenges. Interdiffusion between metal supports and Ni-containing anodes during the high-temperature processing steps and operation of the cell can cause formation of insulating oxides, which leads to the performance degradation. Insertion of a diffusion barrier layer between the support and the anode was shown to help solve the interdiffusion issue. Another difficulty is related to the cathode selection, since the cathode is supposed to be sintered in reducing atmosphere or at the temperature below 900 °C to avoid oxidation of the metal support, while the commonly used cathode materials require sintering in air at 1000–1200 °C to achieve high performance. Largely because of this, the cathode performance in the metal-supported SOFCs often needs improvement. Moreover, such issues as nickel coarsening, carbon deposition, chromium poisoning, and sulfur poisoning restrict the performance and lifetime of the metal-supported SOFCs. In spite of the open challenges, the metal-supported SOFCs are a promising type of fuel cells to use as auxiliary power units and as a power source for mobile apparatus.

6. SOFCs with a freestanding electrolyte film

The issues related to the diffusional interaction between the film and support materials can be avoided in SOFCs with a freestanding thin film electrolyte. A freestanding film is typically fabricated on Si wafers possessing extremely low surface roughness, which allows for uniform depositing of very thin films. After the film deposition, the silicon substrate is removed by lithography and etching to leave the freestanding film. To complete a fuel cell, an anode and a cathode are deposited on the free surfaces of the electrolyte. For the film deposition, such technologies as direct-current (DC) and radio-frequency (RF) sputtering, pulsed laser deposition (PLD) and atomic layer deposition (ALD) are used.

The possibility of fabrication of freestanding films of YSZ electrolyte using the ALD method was reported in [144]. The films were deposited on a Si3N4 buffer layer on Si(100) substrates. Prior to depositing, a Si3N4 buffer layer was patterned to fabricate open window structures. After YSZ deposition, the patterned windows were etched in KOH, leaving freestanding YSZ film and silicon nitride squares with dimensions of tens of micrometers. The Si3N4 layer was removed by plasma assisted chemical etching using SF6 gas, leaving freestanding YSZ layers. The microstructure of the freestanding films consisted of grains of tens of nanometers in diameter. To evaluate the electrical conductivity, porous platinum electrodes were deposited on both sides of the freestanding 60 nm film using DC sputtering (see Figure 14). Testing of the single cell in a SOFC regime demonstrated good performance: a maximum power density of 270 mW cm^{-2} was observed at 350 °C, which was explained by low electrolyte resistance and fast electrode kinetics.

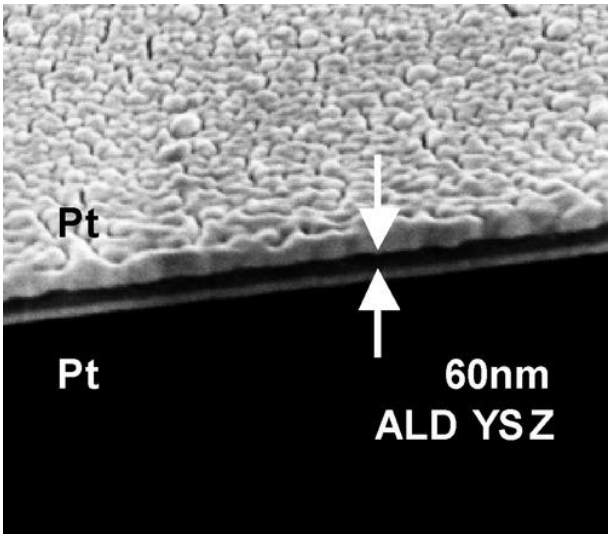

Figure 14 Cross-sectional SEM image of freestanding YSZ films deposited by ALD with porous Pt cathode and anode layers [144].

Another PVD technique – pulsed laser deposition (PLD) – was used for fabrication of freestanding films of YSZ electrolyte by Garbayo et al. [145]. The films with the thickness ranging from 60 to 240 nm and window areas ranging from 50 × 50 μm² to 820 × 820 μm² on silicon-based substrates were obtained. After the film deposition, the SiO2 layer was removed using wet etching in HF solution. It was shown that high quality films could be obtained (yield > 90%) at the deposition temperatures ranging from 200 to 700 °C, while yield dropped considerably for membranes deposited at 800 °C. According to the authors, the drop was caused by high tensile residual stress. The residual stresses in the YSZ membranes deposited by PLD were shown to be significant but tunable by means of post-annealing. For electrical characterization, two symmetrical Pt electrodes were deposited by DC sputtering on the opposite faces of the freestanding films. The electrical conductivity of the films was shown to be similar to the conductivity of bulk YSZ.

Manufacturing and testing of a micro-solid oxide fuel cell with 80 nm thick freestanding YSZ electrolyte membrane deposited by ALD with improved mechanical stability was reported by Baek et al. [146]. The square freestanding Si-supported membrane, fabricated by combining ion etching and wet etching processes, had thicker edges and corners compared to the center part, enhancing the cell mechanical stability. 100 nm thick platinum electrodes were deposited by radio frequency sputtering. The fuel cell was tested upon supply of dry hydrogen as a fuel and air as an oxidant. High values of OCV (1.04 V at 350 °C for more than 30 h of operation) and peak power density (317 mW/cm² at 400 °C) were obtained.

Despite the high power density of the SOFCs with a freestanding thin electrolyte, which was reported in [144, 146], the absolute power output was low because of the small active area. Su et al. [147] applied an advanced method to increase the SOFC effective surface area by manufacturing corrugated YSZ films. The corrugated films were fabricated on silicon templates with the target geometry by ALD method. After deposition, the silicon substrate was partially removed, leaving a freestanding YSZ membrane as shown in Figure 15.

The authors revealed that pinhole free membranes could be fabricated only if the shaped substrate had no sharp corners and the surface roughness was less than the film thickness. A fuel cell with a 70 nm thick YSZ membrane and 120 nm thick porous Pt electrodes deposited by DC magnetron sputtering on both sides of the freestanding membrane was successfully fabricated and tested. The membrane surface was 600 × 600 μm²; the size of the cups was 15 μm in diameter and 20 μm in depth. The peak power density was as high as 861 mW cm⁻² at 450 °C due to the increased effective surface.

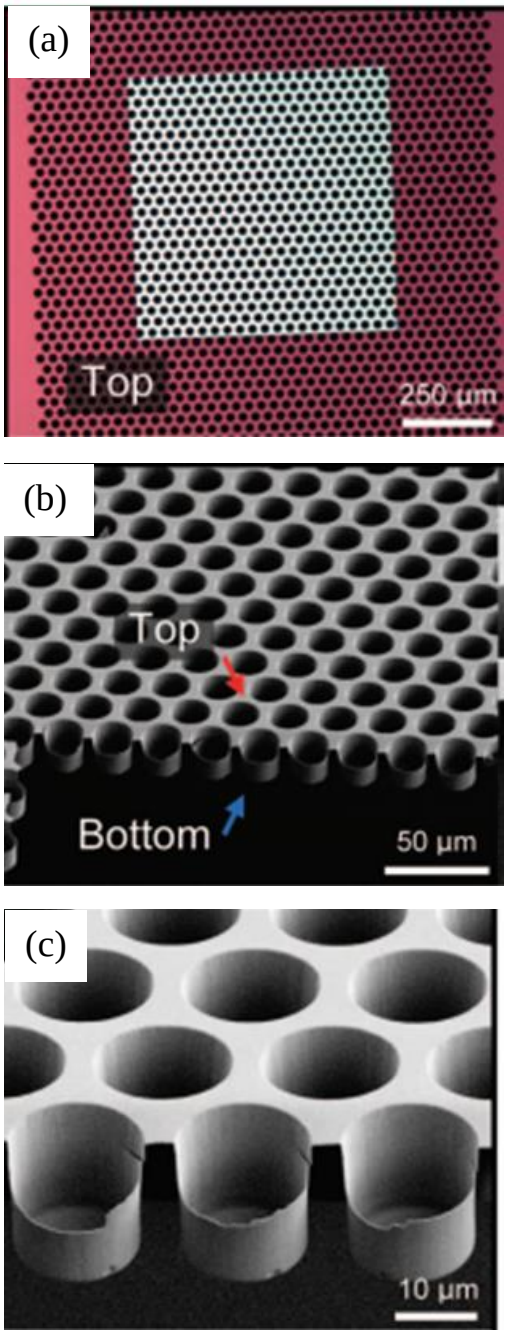

Figure 15 Images of the corrugated YSZ membrane: (a) optical microscopy image of freestanding corrugated YSZ membrane; the white square is the freestanding YSZ membrane released after KOH etching; (b,c) cross-sectional images of cups in the corrugated membrane [146].

It is obvious that the electrolyte thickness must be minimized to reduce the ohmic resistance of a SOFC. However, the freestanding membrane must be free from pinholes or cracks to avoid electrical current leakage and the related decrease in the cell performance. Moreover, the membrane must be thick enough to withstand dielectric breakdown; the calculated minimum thickness of YSZ membrane should be approximately 6 nm to avoid the breakdown [148]. Finally, the membrane loses its mechanical strength with decreasing thickness. Therefore, the membrane must have an optimum thickness to satisfy the above requirements. The reported thickness values of the freestanding YSZ membranes which demonstrate acceptable OCV values varies from 50 to 300 nm [144, 148–151]. However, the thermal cycling resistance of freestanding membranes has not been reported to date.

Summarizing the current findings in the area of SOFCs with a freestanding membrane, we should emphasize their undoubted advantages. The thickness of the freestanding membrane can be decreased to several nanometers and its ionic conductivity can be finely tuned by the precise variation of the composition using the ALD method. Thin electrodes can be easily deposited by the vacuum sputtering methods without using high temperature co-sintering processes, which eliminates the issue of the diffusional interaction. The drop in the ohmic losses allows one to decrease the operation temperature of the fuel cell to 350–450 °C. However, the decrease in the SOFC temperature requires the use of expensive platinum electrodes, since the oxide or composite materials possess low electrochemical activity at low temperatures. Moreover, sophisticated fabrication and very high fragility remain critical challenges.

7. Comparative Summary

Table 1 summarizes the types, configurations, and electrochemical performance of the SOFCs with a thin film electrolyte reported in literature. As can be seen, the dense hydrogen permeable metal anode-supported SOFCs with the 1 μm thick proton-conducting electrolyte $BaCe_{0.8}Y_{0.2}O_{3-\delta}$ demonstrate excellent electrochemical characteristics [125,126]. This can be explained by the low ohmic and polarization resistances of the cells due to the possibility of depositing very thin functional layers on the dense supporting anode, as well as the high proton conductivity of the electrolyte. However, the long-term behavior of these cells may be affected by diffusional interaction and thermal expansion mismatch between the ceramic and metal components. Perhaps this is the reason why the long-term testing and degradation study of this type of SOFCs have not been reported.

High power density was attained in the metal-supported cells due to the possibility of decreasing the thicknesses of all functional layers by depositing them on a porous metal support [130,142]. In contrast to the SOFCs with a dense hydrogen permeable supporting anode, the thickness of the membranes deposited onto the porous metal supports varies in the range of several micrometers to tens of micrometers. For this reason, the metal-supported cells operate at higher temperatures (typically 700–800 °C). The metal-supported SOFCs demonstrate superior mechanical stability, thermal cyclability, and faster start-up time compared to the all-ceramic SOFCs. In addition, the use of inexpensive metal substrates allows one to reduce the manufacturing costs. The problem of interdiffusion between the metal support and the functional layers of the fuel cell is effectively solved by insertion of the diffusion barrier layer over the support. However, such issues as the development of more active cathodes, restraining of nickel coarsening, carbon deposition, and chromium and sulfur poisoning still need to be addressed.

Significant technological advances have been achieved in the field of the planar anode-supported SOFCs. The use of ceramic powder-based technologies and vacuum methods for deposition of the functional layers, the appropriate choice of materials and the cell design resulted in excellent electrochemical characteristics of the oxide-conducting anode-supported SOFC [99]. The proton-conducting SOFC with a supporting anode, fabricated by the technologically simple and cost-effective ceramic powder-based methods, demonstrated very good power generation performance, in spite of the rather thick membrane layer (35 μm) [96].

The microtubular SOFCs have a great potential for portable applications due to fast start-up, small size, and high electrochemical characteristics reported in multiple studies (see e.g. [112–119]). However, the degradation of the cells during the long-term operation remains a weak point.

Much effort has gone into developing SOFC technology and increasing market penetration; however, further efforts need to be made to developing SOFCs with faster start-up and shut-down times and longer lifespan.

Table 1 – Electrochemical performance of different types of SOFCs with a thin film electrolyte.

Components of SOFC, thickness, deposition technology	Testing conditions: temperature, fuel gas, oxidizing gas	OCV, V	PPD, mW cm^{-2}	Ref.
Planar anode-supported SOFCs				
Electrolyte: $SrZr_{0.5}Ce_{0.4}Y_{0.1}O_{3-\delta}$ (SZCY), 16 μm, tape-casting **Anode:** Ni–SZCY, 400 μm, tape-casting **Cathode:** $BaCo_{0.4}Fe_{0.4}Zr_{0.1}Y_{0.1}O_{3-\delta}$, 35 μm, screen-printing	600 °C H_2 + 5% H_2O Air	1.18	170	95
Electrolyte: $Ba(Ce_{0.7}Zr_{0.1}Y_{0.2})O_{3-\delta}$ (BCZY) + 2% NiFe, 35 μm, dip-coating **Anode:** Ni–$Ba_{0.96}(Ce_{0.66}Zr_{0.1}Ni_{0.04}Y_{0.2})O_{3-\delta}$, pressing and sintering **Cathode:** $La_{0.6}Sr_{0.4}Co_{0.2}Fe_{0.8}O_{3-\delta}$ (LSCF)–BCZY, 40 μm, paint brushing	700 °C Hydrogen Air	–	973	96
Electrolyte: $BaCe_{0.4}Zr_{0.4}Y_{0.1}Yb_{0.1}O_{3-\delta}$, (BCZYY), 20 μm, dip-coating **Anode:** Ni– BCZYY, 1 mm, dry pressing **Cathode:** $BaCo_{0.4}Fe_{0.4}Zr_{0.1}Y_{0.1}O_{3-\delta}$, 20 μm, paint brushing	600 °C Hydrogen Air	~1	690 (3-cell stack)	97
Electrolyte: YSZ, 10 μm, EPD **Anode:** Ni–YSZ, slip-casting **Cathode:** $La_{0.8}Sr_{0.2}MnO_{3-\delta}$–YSZ, paint brushing	800 °C Hydrogen Air	1.03	624	98
Electrolyte: bilayer YSZ/$Ce_{0.9}Gd_{0.1}O_{2-\delta}$ (GDC), 4/1.5 μm, reactive pulsed magnetron sputtering **Anode:** Ni-10Sc1YSZ ($(Sc_2O_3)_{0.1}$–$(Y_2O_3)_{0.01}$–$(ZrO_2)_{0.89}$), tape casting **Cathode:** $La_{0.8}Sr_{0.2}CoO_{3-\delta}$, screen-printing	700 °C 800 °C	–	960 1800	99
Electrolyte: bilayer YSZ/GDC, 1/0.3 μm, DC reactive sputtering/RF magnetron sputtering **Anode:** Ni–YSZ, 500 μm, tape-casting/spin-coating **Cathode:** LSCF–GDC, 30 μm, screen-printing	650 °C	–	600	100
Electrolyte: YSZ/GDC, 4/2 μm, reactive magnetron sputtering **Anode:** Ni–YSZ (SOFCMAN, China), 400 μm **Cathode:** LSCF–GDC, 15 μm, screen-printing	750 °C	1.14	470	101
Dense hydrogen permeable metal anode-supported SOFCs				
Electrolyte: $SrZr_{0.8}In_{0.2}O_{3-\delta}$, 0.7–6.0 μm, pulsed laser deposition **Anode:** Pd-foil, 80 μm **Cathode:** LSCF, 30 μm, screen-printing	400 °C Hydrogen Air	1.1	–	124
Electrolyte: $BaCe_{0.8}Y_{0.2}O_{3-\delta}$, 1 μm, RF sputtering **Anode:** Pd-foil, 0.5 mm **Cathode:** LSCF, screen-printing	600 °C Hydrogen Air	1.08	1050	125
Electrolyte: $BaCe_{0.8}Y_{0.2}O_{3-\delta}$, 1 μm, RF sputtering **Anode:** $Pd_{0.8}Ag_{0.2}$-foil, 30 μm **Cathode:** LSCF, screen-printing	600 °C Hydrogen Air	–	1200	126
Microtubular SOFCs				
Supporting anode: Ni-YSZ tube, 0.6 mm thick, phase inversion **Electrolyte:** YSZ, 20 μm, dip-coating **Cathode:** $(La_{0.8}Sr_{0.2})_{0.98}MnO_{3-\delta}$, 30 μm, dip-coating	800 °C H_2 + 3% H_2O Air	~1.1	–	110

Supporting anode: Ni–BZCY tubes, 0.9 mm thick, phase inversion **Electrolyte:** Ba(Zr0.1Ce0.7Y0.2)O3-δ (BZCY), 10 μm, vacuum slurry coating **Cathode:** LSCF–BZCY, 30 μm, dip-coating	700 °C H2 + 5% H2O Air	1.01	500	112
Supporting electrolyte: YSZ, 10 μm, phase inversion **Anode:** Cu-CeO2, vacuum-assisted co-impregnation **Cathode:** LSM, paint brushing	700 °C Dry hydrogen Air	1.19	400	114
Supporting anode: 50 wt% NiO-50 wt% Ce0.8Gd0.2O1.95, 350 μm, dip coating **Electrolyte:** Ce0.8Gd0.2O1.95, 15 μm, dip coating **Cathode:** La0.8Sr0.2Co0.2Fe0.8O3-δ, 40 μm, dip coating	500 °C Hydrogen humidified at room temperature Air	~1	300	116
Supporting anode: NiO-YSZ, phase inversion **Electrolyte:** YSZ, 22 μm, dip coating **Cathode:** La0.6Sr0.4Co0.2Fe0.8O3-δ (LSCF), 6 μm, dip coating	750 °C Hydrogen Air	1.1	1000	117
Supporting anode: Ni–YSZ, Ni–ScSZ, 400 μm, 15 μm, dip coating **Electrolyte:** ScSZ, Sm-doped CeO2, 10 μm, 2 μm, dip coating **Cathode:** LSCF, 20 μm, dip coating	800 °C Hydrogen Air	~1.2	690	118
Supporting anode: NiO–YSZ, 285 μm, cold isostatic pressing **Electrolyte:** YSZ, 15 μm, spraying **Cathode:** (La0.8Sr0.2)0.98MnO3, 40 μm, dip-coating	872 °C Hydrogen Air	>1.1	~600 after 650 h testing	119
Metal-supported SOFCs				
Support: porous stainless-steel (Cr26-Fe), 0.8 mm thick, porosity 40%, powder-metallurgical process Diffusion barrier layer (DBL): GDC, 500 nm, magnetron sputtering **Anode:** Ni-YSZ, 40 μm, screen-printing **Electrolyte:** YSZ, 4 μm, gas-flow sputtering **Cathode:** LSCF, 40 μm, screen-printing	800 °C H2 + 3% H2O Air	–	1000	130
Support: porous stainless-steel/ YSZ-La-doped SrTiO3, tape-casting and lamination **Electrolyte:** YSZ, 2 μm, pulsed laser deposition **Anode:** Ni-YSZ, 0.6 μm, pulsed laser deposition **Cathode:** La0.7Sr0.3CoO3-δ, 0.7 μm, pulsed laser deposition	550 °C H2 + 3% H2O Air	1.05	560	133
Support: porous Ni **Anode:** YSZ/Ni, 10–20 μm, atmospheric plasma spraying **Electrolyte:** La0.8Sr0.2Ga0.8Mg0.2O3-δ, 50–60 μm, atmospheric plasma spraying **Cathode:** La0.58Sr0.4Co0.2Fe0.8O3-δ, 20–30 μm, atmospheric plasma spraying	700 °C 800 °C	>1	170 440	134
Support: porous Ni–Al, combustion synthesis **Anode:** YSZ/Ni, 40 μm, screen-printing **Electrolyte:** YSZ, 25 μm, reactive magnetron sputtering followed by pulsed electron beam treatment **Cathode:** LSCF, 15 μm, screen-printing	800 °C Dry hydrogen Air	>1	360	137
Support: porous stainless-steel, 200 μm, tape-casting **Electrolyte:** (Sc2O3)0.1–(CeO2)0.01–(ZrO2)0.89, 7 μm, tape-casting **Anode:** Sm-doped ceria-40% Ni, 25 μm, infiltration **Cathode:** PrOx, 25 μm, infiltration	700 °C Hydrogen Air	–	1560	142

Support: dense Fe22Cr, 150 μm **Electrolyte:** Sc-doped YSZ (ScYSZ), 10 μm, tape-casting **Anode:** ScYSZ-Fe22Cr, 15 μm, tape-casting **Cathode:** ScYSZ-Fe22Cr, 15 μm, tape-casting	780 °C Dry hydrogen Oxygen	1.07	470	143
SOFCs with a freestanding electrolyte film				
Electrolyte: flat YSZ film, 60 nm, ALD **Anode:** Pt, DC sputtering **Cathode:** Pt, DC sputtering	350 °C	–	270	144
Electrolyte: flat YSZ film, 80 nm, ALD **Anode:** Pt, 100 nm, RF sputtering **Cathode:** Pt, 100 nm, RF sputtering	400 °C	1.04	317	146
Electrolyte: corrugated YSZ film, 70 nm, ALD **Anode:** Pt, 120 nm, DC magnetron sputtering **Cathode:** Pt, 120 nm, DC magnetron sputtering	450 °C	–	861	147

8. Conclusions and Outlook

SOFCs with a thin film electrolyte have significant advantages over the electrolyte-supported SOFCS, including reduced operating temperature, higher stability to thermal cycling and redox cycling, and potentially longer lifespan. In the last decades, notable progress has been made towards the improvement of thin film SOFCs; however, serious challenges still remain. This review article summarizes the configurations, geometries, fabrication technologies, and the obtained characteristics of the thin film SOFCs currently in use, emphasizing the advantages and the current challenges in manufacturing technologies and design strategies, as well as their effect on the electricity generation performances. The review will hopefully contribute to the further development and commercialization of SOFCs with a thin film electrolyte.

Supplementary materials

No supplementary materials are available.

Funding

This research had no external funding.

Acknowledgments

None.

Conflict of interest

The authors declare no conflict of interest.

Additional information

Liliya Dunyushkina (Dr.Sc.) graduated from Department of Physics of the Ural State University named by M. Gorky (Sverdlovsk, USSR) in 1990. She earned her PhD degree in Physical Chemistry from the same university in 1995. Since 2017, she has held a Doctor of Science degree at the Institute of High Temperature Electrochemistry. She has been working as a senior and leading researcher at the Institute of High Temperature Electrochemistry since 1995. Research Interests: transport properties of ionic systems, dynamics of interface processes, electrochemical generation of energy, optimization of electrolyte and electrode materials, chemical solution deposition of solid-oxide films.

References

1. Wang SY, Jiang SP, Prospects of fuel cell technologies, National Science Review, **4** (2017) 163–166. https://doi.org/10.1093/nsr/nww099

2. Trapeznikov AN, Shaikhatdinov FA, Khokhonov AA, Agarkov DA, et al., Obzor kharakteristik toplivnyh elementov izgotavlivaemyh i primenyaemyh na avtomobilnom transporte v Rossii [Overview of characteristics of fuel cells manufactured and applied on motor transport in Russia], Uspekhi v Khimii i Khimicheskoi Tekhnologii, **XXXIV (12)** (2020) 43–46.

3. Jiang SP, Challenges in the development of reversible solid oxide cell technologies: a mini review, Asia Pac. J. Chem. Eng., **11** (2016) 386–391. https://doi.org/10.1002/apj.1987

4. Stambouli AB, Traversa E, Solid oxide fuel cells (SOFCs): a review of an environmentally clean and efficient source of energy, Renew. Sustain. Energy Rev., **6** (2002) 433–455. https://doi.org/10.1016/S1364-0321(02)00014-X

5. Brett DJL, Atkinson A, Brandon NP, Skinner SJ, Intermediate temperature solid oxide fuel cells, Chem. Soc. Rev., **37** (2008) 1568–1578. https://doi.org/10.1039/B612060C

6. Boldrin P, Brandon NP, Progress and outlook for solid oxide fuel cells for transportation applications, Nature Catalysis, **2** (2019) 571–577. https://doi.org/10.1038/s41929-019-0310-y

7. Singh M, Zappa D, Comini E, Solid oxide fuel cell: Decade of progress, future perspectives and challenges, Int. J. Hydrogen Energy, **46** (2021) 27643–27674. https://doi.org/10.1016/j.ijhydene.2021.06.020\

8. Escudero MJ, Yeste MP, Cauqui MA, Muñoz MA, Performance of a direct methane solid oxide fuel cell using nickel-ceria-yttria stabilized zirconia as the anode, Materials, **13** (2020) 599. https://doi.org/10.3390/ma13030599

9. Sengodan S, Lan R, Humphreys J, Du D, et al., Advances in reforming and partial oxidation of hydrocarbons for hydrogen production and fuel cell applications, Renewable and Sustainable Energy Reviews, **82** (2018) 761–780. http://dx.doi.org/10.1016/j.rser.2017.09.071

10. Fischer F, Hauser M, Hauck M, Herrmann S, et al., Effect of internal hydrocarbon reforming during coupled operation of a biomass gasifier with hot gas cleaning and SOFC stacks, Energy Sci Eng., **7** (2019) 1140–1153. https://doi.org/10.1002/ese3.334

11. van Biert L, Godjevac M, Visser K, Aravind PV, Dynamic modelling of a direct internal reforming solid oxide fuel cell stack based on single cell experiments, Applied Energy, **250** (2019) 976-990. https://doi.org/10.1016/j.apenergy.2019.05.053

12. Golkhatmi SZ, Asghar MI, Lund PD, A review on solid oxide fuel cell durability: Latest progress, mechanisms, and study tools, Renew. Sustain. Energy Rev., **161** (2022) 112339. https://doi.org/10.1016/j.rser.2022.112339

13. Mahato N, Banerjee A, Gupta A, Omar S, et al., Progress in material selection for solid oxide fuel cell technology: a review, Prog. Mater. Sci., **72** (2015) 141–337. https://doi.org/10.1016/j.pmatsci.2015.01.001

14. Zhang J, Ricote S, Hendriksen PV, Chen Y, Advanced materials for thin-film solid oxide fuel cells: recent progress and challenges in boosting the device performance at low temperatures, Adv. Funct. Mater., **32** (2022) 2111205. https://doi.org/10.1002/adfm.202111205

15. Sun C, Hui R, Roller J, Cathode materials for solid oxide fuel cells: a review, J. Solid State Electrochem., **14** (2010) 1125–1144. https://doi.org/10.1007/s10008-009-0932-0

16. Vinoth Kumar R, Khandale AP, A review on recent progress and selection of cobalt-based cathode materials for low temperature-solid oxide fuel cells, Renewable and Sustainable Energy Reviews, **156** (2022). https://doi.org/10.1016/j.rser.2021.111985

17. Zakaria Z, Hassan SHA, Shaari N, Yahaya AZ, et al., A review on recent status and challenges of yttria stabilized zirconia modification to lowering the temperature of solid oxide fuel cells operation, Int. J. Energy Res., **44** (2020) 631–650. https://doi.org/10.1002/er.4944

18. Bieberle-Hütter A, Beckel D, Infortuna A, Muecke UP, et al., A micro-solid oxide fuel cell system as battery replacement, Journal of Power Sources, **177** (2008) 123–130. https://doi.org/10.1016/j.jpowsour.2007.10.092

19. Wang HK, Alfred JS, Thangadurai V, Trends in electrode development for next generation solid oxide fuel cells, J. Mater. Chem. A, **4** (2016) 17913–17932. https://doi.org/10.1039/C6TA06757C

20. Nakamura A, Wagner JB, Defect structure, ionic conductivity, and diffusion in yttria stabilized zirconia and related oxide electrolytes with fluorite structure, J. Electrochem. Soc., **133** (1986) 1542–1545.

21. Ioffe AI, Rutman DS, Karpachov SV, On the nature of the conductivity maximum in zirconia-based solid electrolytes, Electrochimica Acta, **23** (1978) 141–142.

22. Atkinson A, Barnett S, Gorte RJ, Irvine JTS, et al., Advanced anodes for high-temperature fuel cells, Nat. Mater., **3** (2004) 17–27. https://doi.org/10.1038/nmat1040

23. da Silva FS, de Souza TM, Novel materials for solid oxide fuel cell technologies: A literature review, Int. J. Hydrogen Energy, **42** (2017) 26020–26036. http://dx.doi.org/10.1016/j.ijhydene.2017.08.105

24. Kan WH, Thangadurai V, Challenges and prospects of anodes for solid oxide fuel cells (SOFCs), Ionics, **21** (2015) 301–318. https://doi.org/10.1007/s11581-014-1334-6

25. Liu Y, Shao Z, Mori T, Jiang SP, Development of nickel based cermet anode materials in solid oxide fuel cells – now and future, Materials Reports: Energy, **1** (2021) 100003. https://doi.org/10.1016/j.matre.2020.11.002

26. Faes A, Hessler-Wyser A, Zryd A, Van herle J, A review of redox cycling of solid oxide fuel cells anode, Membranes **2** (2012) 585–664. https://doi.org/10.3390/membranes2030585

27. Tarancon A, Strategies for lowering solid oxide fuel cells operating temperature, Energies, **2** (2009) 1130–1150. https://doi.org/10.3390/en20401130

28. Ndubuisi A, Abouali S, Singh K, Thangadurai V, Recent advances, practical challenges, and perspectives of intermediate temperature solid oxide fuel cell cathodes, J. Mater. Chem. A, **10** (2022) 2196–2227. https://doi.org/10.1039/d1ta08475e

29. Katsuki M, Wang S, Dokiya M, Hashimoto T, High temperature properties of La0.6Sr0.4Co0.8Fe0.2O3- δ : oxygen nonstoichiometry and chemical diffusion constant, Solid State Ionics, **156** (2003) 453–461. https://doi.org/10.1016/S0167-2738(02)00733-6

30. Lane JA, Benson SJ, Waller D, Kilner JA, Oxygen transport in La0.6Sr0.4Co0.2Fe0.8O3- δ , Solid State Ionics, **121** (1999) 201–208.

31. Ishigaki T, Yamaguchi S, Mizusaki J, Fueki K, Tracer diffusion coefficient of oxide ions in LaCoO3 single crystal, Journal of Solid State Chemistry, **54** (1984) 100–107.

32. de Souza RA, Kilner JA, Oxygen transport in La-Sr-Mn-Co-O perovskites, Solid State Ionics, **126** (1999) 153–161.

33. Jiang SP, Development of lanthanum strontium cobalt ferrite perovskite electrodes of solid oxide fuel cells – A review. Int. J. Hydrogen Energy, **44** (2019) 7448–7493. https://doi.org/10.1016/j.ijhydene.2019.01.212

34. Boehm E, Bassat JM, Dordor P, Mauvy F, et al., Oxygen diffusion and transport properties in non-stoichiometric Ln2-xNiO4+□ oxides, Solid State Ionics, **176** (2005) 2717–2725. https://doi.org/10.1016/J.SSI.2005.06.033

35. Kilner JA, Shaw CKM, Mass transport in La2Ni1-xCoxO4+d oxides with the K2NiF4 structure, Solid State Ionics, **154–155** (2002) 523–527. http://dx.doi.org/10.1016/S0167-2738(02)00506-4

36. Ding P, Li W, Zhao H, Wu C, et al., Review on Ruddlesden–Popper perovskites as cathode for solid oxide fuel cells, J. Phys. Mater. **4** (2021) 022002. https://doi.org/10.1088/2515-7639/abe392

37. Tang H, Jin Z, Wu Y, Liu W, Bi L, Cobalt-free nanofiber cathodes for proton conducting solid oxide fuel cells, Electrochemistry Communications, **100** (2019) 108–112. https://doi.org/10.1016/j.elecom.2019.01.022

38. Tarutin AP, Lyagaeva JG, Medvedev DA, Bi L, et al., Recent advances in layered Ln2NiO4+d nickelates: fundamentals and prospects of their applications in protonic ceramic fuel and electrolysis cells, Journal of Materials Chemistry A, **9 (1)** (2021) 154–195. http://dx.doi.org/10.1039/d0ta08132a

39. Hodjati-Pugh O, Dhir A, Steinberger-Wilckens R, The development of current collection in micro-tubular solid oxide fuel cells – a review, Appl. Sci., **11** (2021) 1077. https://doi.org/10.3390/app11031077

40. Kuterbekov KA, Nikonov AV, Bekmyrza KZ, Pavzderin NB, et al., Classification of solid oxide fuel cells, Nanomaterials, **12** (2022) 1059. https://doi.org/10.3390/nano12071059

41. Su PC, Chao CC, Shim JH, Fasching R, et al., Solid oxide fuel cell with corrugated thin film electrolyte, Nano Lett., **8** (2008) 2289–2292. https://doi.org/10.1021/nl800977z

42. Khan MZ, Iltaf A, Ishfaq HA, Khan FN, et al., Flat-tubular solid oxide fuel cells and stacks: a review, Journal of Asian Ceramic Societies, **9 (3)** (2021) 745–770. https://doi.org/10.1080/21870764.2021.1920135

43. Lemański M, Topolski J, Badur J. Analysis strategies for gas turbine – solid oxide fuel cell hybrid cycles. Technical, economic, and environmental aspects of combined cycle power plants. Gdańsk: TU Press; 2004. 213–220.

44. Powell R, Rossnagel S. PVD for microelectronics: sputter deposition applied to semiconductor manufacturing. Academic Press; 1999. 419 p.

45. Yang Y, Zhang Y, Yan M, A review on the preparation of thin-film YSZ electrolyte of SOFCs by magnetron sputtering technology, Separation and Purification Technology, **298** (2022) 121627. https://doi.org/10.1016/j.seppur.2022.121627

46. Snowdon AL, Jiang Z, Steinberger-Wilckens R, Five-layer reverse tape-casting of IT-SOFC, Int. J. Appl. Ceram. Technol., **19** (2022) 289–298. https://doi.org/10.1111/ijac.13911

47. Pierson HO. Handbook of chemical vapor deposition (CVD): principles, technology and applications. N.J.: Noyes Publications; 1992. 436 p.

48. Dunyushkina LA. Vvedeniye v metody polucheniya plyonochnykh elektrolitov dlya tvyordooksidnykh toplivnykh elementov [Introduction into deposition methods of film electrolytes for solid oxide fuel cells]. Ekaterinburg: Publishing and Printing Center of Ural Federal University; 2015. 128 p. Russian.

49. Abegunde OO, Akinlabi ET, Oladijo OP, Akinlabi S, et al., Overview of thin film deposition techniques, AIMS Materials Science, **6 (2)** (2019) 174–199. https://doi.org/10.3934/matersci.2019.2.174

50. Jaeger RC. Film deposition. Introduction to microelectronic fabrication. 2nd ed. Upper Saddle River: Prentice Hall; 2002. 316 p.

51. Semiconductor Devices: Physics and Technology. Ed.: Sze SM. NY: John Wiley; 1969. 812 p.

52. Kuzmichev A, Tsybulsky L. Evaporators with induction heating and their applications. Advances in induction and microwave heating of mineral and organic materials. Ed.: Grundas S. InTech; 2011. – 766 p.

53. Laukaitis G, Dudonis J, Milcius D, Morphology and growth of e-beam deposited YSZ thin films, Vacuum, **81** (2007) 1288–1291. https://doi.org/10.1016/j.vacuum.2007.01.030

54. Laukaitis G, Dudonis J, Milcius D, Microstructure and surface morphology of YSZ thin films deposited by e-beam technique, Applied Surface Science, **254** (2008) 2980–2987. https://doi.org/10.1016/j.apsusc.2007.10.041

55. He X, Meng B, Sun Y, Liu B, Li M, Electron beam physical vapor deposition of YSZ electrolyte coatings for SOFCs, Applied Surface Science, **254** (2008) 7159–7164. https://doi.org/10.1016/j.apsusc.2008.05.271

56. Yang S, Kim K, Choi H, The properties of Co- and Fe-doped GDC for low-temperature processing of solid oxide fuel cell by electron-beam evaporation, Journal of Nanoscience and Nanotechnology, **8** (2013) 5794–5799. https://doi.org/10.1166/jnn.2013.7562

57. Suh JH, Kim HS, Park CG. Interfacial structure and crystallinity of YSZ thin films grown by ion beam sputtering for MFIS-FRAM. In: IEEE Nanotechnology Materials and Devices Conference Vol. 1; 2006 Oct 22–25; Gyeongju, South Korea. p. 702. https://doi.org/10.1109/NMDC.2006.4388969

58. Chen YJ, Wei WC. Investigation of YSZ thin films on silicon wafer and NiO/YSZ deposited by ion beam sputtering deposition (IBSD). Key Engineering Materials, **336–338** (2007) 1788–1790. https://doi.org/10.4028/www.scientific.net/kem.336-338.1788

59. Sønderby S, Nielsen AJ, Christensen BH, Almtoft KP, et al., Reactive magnetron sputtering of uniform yttria-stabilized zirconia coatings in an industrial setup, Surface & Coatings Technology, **206** (2012) 4126–4131. https://doi.org/10.1016/j.surfcoat.2012.04.007

60. Kuo YL, Lin SE, Wei WCJ, Su YM, Sputter-deposited 20 mol% gadolinia-doped ceria films on 8 mol% yttria-stabilized zirconia tapes for improved electrochemical performance, Thin Solid Films, **618** (2016) 202–206. https://doi.org/10.1016/j.tsf.2016.03.009

61. Coddeta P, Caillard A, Vulliet J, Richard C, et al., Multistep magnetron sputtering process and in-situ heat treatment to manufacture thick, fully oxidized and well crystallized YSZ films, Surface and Coatings Technology, **349** (2018) 133–143. https://doi.org/10.1016/j.surfcoat.2018.05.065

62. Bobrenok OF, Predtechenskii MR, Solid oxide fuel cells with film electrolytes prepared by chemical vapor deposition, Russian Journal of Electrochemistry, **46 (7)**

(2010) 798–804. https://doi.org/10.1134/S102319351007013X

63. Hou X, Choy K-L, Processing and applications of aerosol-assisted chemical vapor deposition, Chem. Vap. Deposition, **12** (2006) 583–596. https://doi.org/10.1002/cvde.200600033

64. Perednis D. Thin Film Deposition by Spray Pyrolysis and the Application in Solid Oxide Fuel Cells [Dissertation]. Zurich (Switzerland); 2003. 166 p.

65. Vervaele M, Roo BD, Deschaume O, Rajala M, et al., Development of a new direct liquid injection system for nanoparticle deposition by chemical vapor deposition using nanoparticle solutions, Review of Scientific Instruments, **87** (2016) 025101. https://doi.org/10.1063/1.4940937

66. Aleskovskii VB. Stekhiometriya i sintez tverdykh soedinenii [Stoichiometry and synthesis of solid compounds]. Leningrad: Nauka; 1976. 140 p. Russian.

67. Suntola T. Atomic Layer Epitaxy // In Handbook of Crystal Growth. V. 3. / Edited by Hurle D.T.J. – Amsterdam: Elsevier, 1994. – P. 601–663.

68. Nishizawa J, Abe H, Kurabayashi T, Molecular layer epitaxy, J. Electrochem. Soc., **132** (1985) 1197.

69. Puurunen RL, Surface chemistry of atomic layer deposition: a case study for the trimethylaluminum/water process, J. Appl. Phys., **97** (2005) 121–301. https://doi.org/10.1063/1.1940727

70. Schwartz RW, Chemical solution deposition of perovskite thin films, Chem. Mater., **9** (1997) 2325–2340.

71. Oh EO, Whang CM, Hwang HJ, Lee YR, Thin film yttria-stabilized zirconia (YSZ) electrolyte fabricated by a novel chemical solution deposition (CSD) process for solid oxide fuel cells (SOFCs), Journal of Nanoelectronics and Optoelectronics, **7 (5)** (2012) 554–558. https://doi.org/10.1166/jno.2012.1377

72. Gadea C, Hanniet Q, Lesch A, Marani D, Aqueous metal–organic solutions for YSZ thin film inkjet deposition, J. Mater. Chem. C, **5** (2017) 6021–6029. https://doi.org/10.1039/c7tc01879g

73. Dunyushkina LA, Khaliullina AS, Kuimov VM , Osinkin DA, et al., Influence of modification of chemical solution deposition on morphology and conductivity of CaZr0.9Y0.1O3- δ films, Solid State Ionics, 329 (2019) 1–7. https://doi.org/10.1016/j.ssi.2018.11.015

74. Zhou J, Zhang L, Liu C, Pu J, et al., Aqueous tape casting technique for the fabrication of Sc0.1Ce0·01Zr0·89O2+ Δ ceramic for electrolyte-supported solid oxide fuel cell, Int. J. Hydrogen Energy, **44** (2019) 21110–21114. https://doi.org/10.1016/j.ijhydene.2019.01.265

75. Goulart C, de Souza D, Critical analysis of aqueous tape casting, sintering, and characterization of planar yttria-stabilized zirconia electrolytes for SOFC, Int. J. Appl. Ceram. Technol., **14** (2017) 413–423. https://doi.org/10.1111/ijac.12638

76. Agarkova EA, Agarkov DA, Burmistrov IN, Zadorozhnay OY, et al., Three-layered membranes for planar solid oxide fuel cells of the electrolyte-supported design: characteristics and applications, Russian Journal of Electrochemistry, **56 (2)** (2020) 132–138. https://doi.org/10.1134/S1023193520020020

77. Kwon Y, Han Y, Fabrication of electrolyte-supported solid oxide fuel cells using a tape casting process, Journal of the Ceramic Society of Japan, **128 (6)** (2020) 310–316. https://doi.org/10.2109/jcersj2.20006

78. Kim J, Kim J, Yoon KJ, Son JW, et al., Solid oxide fuel cells with zirconia/ceria bilayer electrolytes via roll calendering process, Journal of Alloys and Compounds, **846** (2020) 156318. https://doi.org/10.1016/j.jallcom.2020.156318

79. Zhang B, Gong J, Wei K, Yuea S, et al., The instructive role of mechanical properties of polyvinyl alcohol film in the process of YSZ tape calendaring, Ceramics International, **46** (2020) 17010–17017. https://doi.org/10.1016/j.ceramint.2020.03.286

80. Medvedev D, Lyagaeva J, Vdovin G, Beresnev S, et al., A tape calendering method as an effective way for the preparation of proton ceramic fuel cells with enhanced performance, Electrochimica Acta, **210** (2016) 681–688. https://doi.org/10.1016/j.electacta.2016.05.197

81. Somalu MR, Muchtar A, Daud WRW, Brandon NP, Screen-printing inks for the fabrication of solid oxide fuel cell films: a review, Renewable and Sustainable Energy Reviews, **75** (2017) 426–439. http://dx.doi.org/10.1016/j.rser.2016.11.008

82. Zhang Y, Huang X, Lu Z, Liu Z, et al., A study of the process parameters for yttria-stabilized zirconia electrolyte films prepared by screen-printing, Journal of Power Sources, **160 (2)** (2006) 1065–1073. https://doi.org/10.1016/j.jpowsour.2006.02.074

83. Onbilgin S, Timurkutluk B, Timurkutluk C, Celik S, Comparison of electrolyte fabrication techniques on the performance of anode supported solid oxide fuel cells, International Journal of Hydrogen Energy, **45 (60)** (2020) 35162–35170. https://doi.org/10.1016/j.ijhydene.2020.01.097

84. Dollen PV, Barnett SA, A study of screen printed yttria-stabilized zirconia layers for solid oxide fuel cells, Journal of the American Ceramic Society, **88 (12)** (2005) 3361–3368. https://doi.org/10.1111/j.1551-2916.2005.00625.x

85. Ried P, Lorenz C, Bronstrup A, Graule T, et al., Processing of YSZ screen printing pastes and the characterization of the electrolyte layers for anode supported SOFC, Journal of the European Ceramic Society, **28** (2008) 1801–1808. https://doi.org/10.1016/j.jeurceramsoc.2007.11.018

86. Hołda AK, Vankelecom IFJ, Understanding and guiding the phase inversion process for synthesis of solvent resistant nanofiltration membranes, J. Appl. Polym. Sci., **132 (27)** (2015) 42130. https://doi.org/10.1002/app.42130

87. Li N, Wang L, Wang M, Ban X, et al., Ni-cermet with straight pore paths as cathode for solid oxide electrolysis cell enabling energy-efficient and coking-resistant conversion of CO2, Journal of Power Sources **518** (2022) 230787. https://doi.org/10.1016/j.jpowsour.2021.230787

88. Meng X, Yang N, Meng B, Tan X, et al., Microstructure tailoring of the nickel–yttria stabilised zirconia (Ni–YSZ) cermet hollow fibres, Ceramics International, **38 (8)** (2012) 6327–6334. https://doi.org/10.1016/j.ceramint.2012.05.002

89. Ishihara T, Sato K, Takita Y, Electrophoretic deposition of Y2O3-stabilized ZrO2 electrolyte films in solid oxide fuel cells, J. Am. Ceram. Soc., **79 (4)** (1996) 913–919. https://doi.org/10.1111/j.1151-2916.1996.tb08525.x

90. Sarkar P, Huang X, Nicholson PS, Zirconia-alumina functionally-gradiented composites by electrophoretic deposition techniques, J. Am. Ceram. Soc., **76 (4)** (1993) 1055–1056.

91. Meepho M, Wattanasiriwech D, Wattanasiriwech S, Aungkavattana P, Preparation of NiO-YSZ substrate for electrophoretic deposition of thin YSZ film, Energy Procedia, **34** (2013) 714–720. https://doi.org/10.1016/j.egypro.2013.06.804

92. Kalinina E, Pikalova E, Ermakova L, Bogdanovich N, Challenges of formation of thin-film solid electrolyte layers on non-conductive substrates by electrophoretic deposition, Coatings, 11 (2021) 805. https://doi.org/10.3390/coatings11070805

93. Pikalova EY, Kalinina EG, Electrophoretic deposition in the solid oxide fuel cell technology: fundamentals and recent advances, Renew. Sustain. Energy Rev., **116** (2019) 109440. https://doi.org/10.1016/j.rser.2019.109440

94. Parhizkara T, Hafeznezami S, Degradation based operational optimization model to improve the productivity of energy systems, case study: solid oxide fuel cell stacks, Energy Conversion and Management, **158** (2018) 81–91. https://doi.org/10.1016/j.enconman.2017.12.045

95. Leonard K, Ivanova ME, Weber A, Deibert W, et al., Anode supported planar 5 × 5 cm2 SrZr0.5Ce0.4Y0.1O2.95 based solid oxide protonic fuel cells via sequential tape-casting, Solid State Ionics, **379** (2022) 115918. https://doi.org/10.1016/j.ssi.2022.115918

96. Liu Z, Chen M, Zhou M, Cao D, et al., Multiple effects of iron and nickel additives on the properties of proton conducting yttrium-doped barium cerate-zirconate electrolytes for high-performance solid oxide fuel cells, ACS Appl. Mater. Interfaces, **12 (45)** (2020) 50433–50445. https://dx.doi.org/10.1021/acsami.0c14523

97. Le LQ, Hernandez CH, Rodriguez MH, Zhu L, et al., Proton-conducting ceramic fuel cells: Scale up and stack integration, Journal of Power Sources, **482** (2021) 228868. https://doi.org/10.1016/j.jpowsour.2020.228868

98. Majhi SM, Behura SK, S. Bhattacharjee S, Singh BP, et al., Anode supported solid oxide fuel cells (SOFC) by electrophoretic deposition, Int. J. Hydrogen Energy, **36** (2011) 14930–14935. https://doi.org/10.1016/j.ijhydene.2011.02.100

99. Agarkova EA, Burmistrov IN, Agarkov DA, Zadorozhnaya OY, et al., Bilayered anode supports for planar solid oxide fuel cells: fabrication and electrochemical performance, Materials Letters, **283** (2021) 128752, https://doi.org/10.1016/j.matlet.2020.128752

100. Kang S, Lee J, Cho GY, Kim Y, et al., Scalable fabrication process of thin-film solid oxide fuel cells with an anode functional layer design and a sputtered electrolyte, Int. J. Hydrogen Energy, **45** (2020) 33980–33992. https://doi.org/10.1016/j.ijhydene.2020.09.033

101. Solovyev AA, Lebedynskiy AM, Shipilova AV, Ionov IV, et al., Scale-up of solid oxide fuel cells with magnetron sputtered electrolyte, Fuel Cells, 17 (3) (2017) 378–382. https://dx.doi.org/10.1002/fuce.201600227 F

102. Sochugov NS, Soloviev AA, Shipilova AV, Rotshtein VP, An ion-plasma technique for formation of anode-supported thin electrolyte films for IT-SOFC applications, Int. J. Hydrogen Energy, 36 (9) (2011) 5550–5556. https://dx.doi.org/10.1016/j.ijhydene.2011.01.159

103. Kim YJ, Le MC, Evaluation of the thermal and structural stability of planar anode-supported solid oxide fuel cells using a 10 x 10 cm2 single-cell test, Int. J. Hydrogen Energy, **44** (2019) 5517–5529. https://doi.org/10.1016/j.ijhydene.2018.08.099

104. Lin CK, Anam K, Wu SH, Lee RY Simulation of cracking of electrode assembly in planar solid oxide fuel cell, ECS Transactions, **57 (1)** (2013) 2597-2606. https://doi.org/10.1149/05701.2597ecst

105. Zheng J, Xiao L, Wu M, Lang S, et al., Numerical analysis of thermal stress for a stack of planar solid oxide fuel cells. Energies, **15** (2022) 343. https://doi.org/10.3390/en15010343

106. Kalib NS, Muchtar A, Somalu MR, Ihsan AKAM, et al., Influence of heat transfer on thermal stress development in solid oxide fuel cells: a review, Journal of Advanced Research in Fluid Mechanics and Thermal Sciences, **54 (2)** (2019) 175–184.

107. Suzuki T, Improvement of SOFC performance using a microtubular, anode-supported SOFC, J. Electrochem. Soc., **153 (5)** (2006) A925–A928. https://dx.doi.org/10.1149/1.2185284

108. Alston T, Kendall K, Palin M, Prica M, et al., A 1000-cell SOFC reactor for domestic cogeneration, Journal of Power Sources, **71** (1998) 271–274.

109. Du Y, Finnerty C, Jiang J, Thermal stability of portable microtubular SOFCs and stacks, J. Electrochem. Soc., **155** (2008) B972–B977.

110. Monzón H, Laguna-Bercero MA, Highly stable microtubular cells for portable solid oxide fuel cell applications, Electrochimica Acta, **222** (2016) 1622–1627. https://doi.org/10.1016/j.electacta.2016.11.150

111. Zazhigalov SV, Popov MP, Nemudry AP, et al., Mathematical modeling and experimental studies of microtubular solid oxide fuel cells, Theor. Found. Chem. Eng, **54** (2020) 647–654. https://doi.org/10.1134/S0040579520040284

112. Min SH, Song RH, Lee JG, Park MG, et al., Fabrication of anode-supported tubular Ba(Zr0.1Ce0.7Y0.2)O3- δ cell for intermediate temperature solid oxide fuel cells, Ceramics International, **40** (2014) 1513–1518. https://doi.org/10.1016/j.ceramint.2013.07.036

113. Lawlor V, Griesser S, Buchinger G., Olabi AG, et al., Review of the micro-tubular solid oxide fuel cell Part I. Stack design issues and research activities, Journal of Power Sources, **193** (2009) 387–399. https://doi.org/10.1016/j.jpowsour.2009.02.085

114. Rabuni MF, Li T, Punmeechao P, Li K, Electrode design for direct-methane micro-tubular solid oxide fuel cell (MTSOFC), Journal of Power Sources, **384** (2018) 287–294. https://doi.org/10.1016/j.jpowsour.2018.03.002

115. Majewski AJ, Dhir A, Application of silver in microtubular solid oxide fuel cells, Materials for Renewable and Sustainable Energy, **7** (2018) 16. https://doi.org/10.1007/s40243-018-0123-y

116. Villegas CIR, Rendon CLF, Avila-Paredes HJ, Performance evaluation of microtubular solid oxide fuel cell prototypes at a laboratory scale and identification of needs related to gas sensors, Proceedings, **2** (2018) 106. doi:10.3390/ecsa-4-04910

117. Milcarek R, Ahn J, Micro-tubular solid oxide fuel cell polarization and impedance variation with thin porous samarium-doped ceria and gadolinium-doped ceria buffer layer thickness, J. Electrochem. En. Conv.

Stor., **18 (2)** (2021) 021004. https://doi.org/10.1115/1.4047742

118. Sahu SK, Panthi D, Soliman I, Feng H, et al., Fabrication and performance of micro-tubular solid oxide cells, Energies, **15** (2022) 3536. https://doi.org/10.3390/en15103536

119. Laguna-Bercero MA, Férriz A, Larrea A, Correas L, et al., Long-term stability studies of anode-supported microtubular solid oxide fuel cells, Fuel Cells, **13 (6)** (2013) 1116–1122. https://doi.org/10.1002/fuce.201300063

120. Yang NT, Tan XY, Ma ZF, Thursfield A, Fabrication and characterization of Ce0.8Sm0.2O1.9 microtubular dual-structured electrolyte membranes for application in solid oxide fuel cell technology, Journal of The American Ceramic Society, **92 (11)** (2009) 2544–2550. https://doi.org/10.1111/j.1551-2916.2009.03267.x

121. Kovalev IV, Sivcev VP, Guskov PD, Popov MP, et al., A new type of microtubular oxygen permeable membranes fabricated by phase inversion with the use of additive manufacturing technologies, Russian Journal of Electrochemistry, **58** (2022) 585–593. https://doi.org/10.1134/S1023193522070096

122. Popov MP, Bychkov SF & Nemudry AP, Improvement of performance of oxygen-conducting membranes by electric heating, Dokl. Phys. Chem., **478** (2018) 19–22. https://doi.org/10.1134/S0012501618010050

123. Voloshin BV, Bulina NV, Popov MP, Nemudry AP, Operando x-ray diffraction analysis of a microtubular La0.6Sr0.4Co0.2Fe0.8O3– δ membrane, Russian Journal of Electrochemistry, **58 (2)** (2022) 100–104. https://doi.org/10.1134/S1023193522020100

124. Ito N, Aoyama S, Masui T, Matsumoto S, et al., Electrochemical analysis of hydrogen membrane fuel cells, J. Power Sources, **185** (2008) 922–926. https://doi.org/10.1016/j.jpowsour.2008.08.004

125. Aoki Y, Kobayashi S, Yamaguchi T, Tsuji E, et al., Electrochemical impedance spectroscopy of high-efficiency hydrogen membrane fuel cells based on sputter-deposited BaCe0.8Y0.2O3– δ thin films, J. Phys. Chem. C, **120** (2016) 15976–15985. https://doi.org/10.1021/acs.jpcc.5b12593

126. Aoki Y, Yamaguchi T, Kobayashi S, Zhu C, et al., High efficiency hydrogen membrane fuel cells with BaCe0.8Y0.2O3- δ electrolyte thin films and Pd1-xAgx solid anodes, J. Electrochem. Soc., **164 (6)** (2017) F577–F581. https://doi.org/10.1149/2.0661706jes

127. Tucker MC, Progress in metal-supported solid oxide fuel cells: a review, Journal of Power Sources, **195** (2010) 4570–4582. https://doi.org/10.1016/j.jpowsour.2010.02.035

128. Ruhma Z, Yashiro K, Oikawa I, Takamura H, et al., Metal-supported SOFC fabricated by tape casting and its characterization: a study of the co-sintering process, J. Eng. Technol. Sci., **53 (5)** (2021) 210511. https://doi.org/10.5614/j.eng.technol.sci.2021.53.5.11

129. Zhou Z, Nadimpalli VK, Pedersen DB, Esposito V, Degradation mechanisms of metal-supported solid oxide cells and countermeasures: a review, Materials, **14** (2021) 3139. https:// doi.org/10.3390/ma14113139

130. Roehrens D, Packbier U, Fang Q, Blum L, et al., Operation of thin-film electrolyte metal-supported solid oxide fuel cells in lightweight and stationary stacks: material and microstructural aspects, Materials, **9** (2016) 762. https://doi.org/10.3390/ma9090762

131. Kim KJ, Kim SJ, Choi GM, Y0.08Sr0.88TiO3–CeO2 composite as a diffusion barrier layer for stainless-steel supported solid oxide fuel cell, J. Power Sources, **307** (2016) 385–390.

132. Uchiyama K, Isse Y, Hori Y, Nishida T, et al., Structural and electrical characterization of Y-doped SrZrO3 thin films for solid oxide fuel cells. In: Proceeding of 6th Thin Film Materials & Devices Meeting; 2009 November 2-3; Kyoto, Japan, 100228102.

133. Kim KJ, Park BH, Kim SJ, Lee Y, et al., Micro solid oxide fuel cell fabricated on porous stainless steel: a new strategy for enhanced thermal cycling ability, Scientific Reports, **6** (2016) 22443. https://doi.org/10.1038/srep22443

134. Hwang C, Tsai CH, Lo CH, Sun SH, Plasma sprayed metal supported YSZ/Ni–LSGM–LSCF ITSOFC with nanostructured anode, J. Power Sources, **180** (2008) 132–142. https://doi.org/10.1016/j.jpowsour.2008.01.075

135. Sumi H, Shimada H, Yamaguchi Y, Yamaguchi T, Metal-supported microtubular solid oxide fuel cells with ceria-based electrolytes, Journal of the Ceramic Society of Japan, **125 (4)** (2017) 208-212. https://doi.org/10.2109/jcersj2.16221

136. Ishihara T, Yan J, Enoki M, Okada S, et al., Ni–Fe Alloy-Supported Intermediate Temperature SOFCs Using LaGaO3LaGaO3 Electrolyte Film for Quick Startup, J. Fuel Cell Sci. Technol., **5 (3)** (2008) 031205. https://doi.org/10.1115/1.2930763

137. Solovyev AA, Rabotkin SV, Shipilova AV, Kirdyashkin AI, et al., Solid oxide fuel cell with Ni-Al support, Int. J. Hydrogen Energy, **40** (2015) 14077–14084. http://dx.doi.org/10.1016/j.ijhydene.2015.07.151

138. Ju YW, Eto H, Inagaki T, Ishihara T, High power SOFC using LSGM film on NiFe porous bi-metal substrate, ECS Trans. **25 (2)** (2009) 719–726.

139. Vasylechko L, Vashook V, Savytskii D, Senyshyn A, et al., Crystal structure, thermal expansion and conductivity of anisotropic La1–xSrxGa1–2xMg2xO3–y (x=0.05, 0.1) single crystals, Journal of Solid State Chemistry, **172 (2)** (2003) 396-411. https://doi.org/10.1016/S0022-4596(03)00016-1

140. Yu J, Liu H, Chen X, Xing J, et al., Ionic conductivity and crystal structure of LSGM with different element mole ratios, Fuel Cells, **21** (2021) 149–154. https://doi.org/10.1002/fuce.202000056

141. Tucker MC, Kurokawa H, Jacobson CP, De Jonghe LC, et al., A fundamental study of chromium deposition on solid oxide fuel cell cathode materials, **160 (1)** (2006) 130–138. https://doi.org/10.1016/j.jpowsour.2006.02.017

142. Dogdibegovic E, Wang R, Lau GY, Tucker MC, High performance metal-supported solid oxide fuel cells with infiltrated electrodes, Journal of Power Sources, **410–411** (2019) 91–98. https://doi.org/10.1016/j.jpowsour.2018.11.004

143. Pirou S, Talic B, Brodersen K, Hauch A, et al., Production of a monolithic fuel cell stack with high power density, Nature Communications, **13** (2022) 1263. https://doi.org/10.1038/s41467-022-28970-w

144. Shim JH, Chao CC, Huang H, Prinz FB, Atomic layer deposition of yttria-stabilized zirconia for solid oxide fuel cells, Chem. Mater., **19** (2007) 3850–3854. https://doi.org/10.1021/cm070913t

145. Garbayo I, Tarancón A, Santiso J, Cavallaro A, et al., Fabrication and characterization of yttria-stabilized zirconia membranes for micro solid oxide fuel cells. In: Proc. of SPIE - Smart Sensors, Actuators, and MEMS IV; 2009 May 18; Dresden, Germany edited by Ulrich Schmid, Carles Cané, Herbert Shea. V. 7362, 73621B-1. https://doi.org/10.1117/12.821613

146. Baek JD, Yu CC, Su PC, A silicon-based nanothin film solid oxide fuel cell array with edge reinforced support for enhanced thermal mechanical stability, Nano Lett., **16** (2016) 2413–2417.

https://doi.org/10.1021/acs.nanolett.5b05221

147. Su PC, Chao CC, Shim JH, Fasching R., et al., Solid oxide fuel cell with corrugated thin film electrolyte, Nano Letters **8 (8)** (2008) 2289–2292. https://doi.org/10.1021/nl800977z

148. Kerman K, Ramanathan S, Performance of solid oxide fuel cells approaching the two-dimensional limit, J. Appl. Phys., **115** (2014) 174307. https://doi.org/10.1063/1.4874738

149. Huang H, Nakamura M, Su PC, Fasching R, et al., High-performance ultrathin solid oxide fuel cells for low-temperature operation, J. Electrochem. Soc., **154** (2007) B20–B24. https://doi.org/10.1149/1.2372592

150. Jiang XR, Huang H, Prinz FB, Bent SF, Application of atomic layer deposition of platinum to solid oxide fuel cells, Chem. Mater., **20** (2008) 3897–3905. https://doi.org/10.1021/cm7033189

151. Evans A, Martynczuk J, Stender D, Schneider CW, et al., Low-temperature micro-solid oxide fuel cells with partially amorphous La0.6Sr0.4CoO3- δ cathodes, Adv. Energy Mater., **5** (2015) 1400747. https://doi.org/10.1002/aenm.201400747